Saudi Pharmaceutical Journal 30 (2022) 1572–1588

HOSTED BY

Contents lists available at ScienceDirect

Saudi Pharmaceutical Journal

journal homepage: www.sciencedirect.com

Original article

Mechanism of action of *Orthosiphon stamineus* against non-alcoholic fatty liver disease: Insights from systems pharmacology and molecular docking approaches

Salah Abdulrazak Alshehade [a,b], Raghdaa Hamdan Al Zarzour [a,c,*], Vikneswaran Murugaiyah [a], Sharoen Yu Ming Lim [d], Huda Ghaleb El-Refae [e], Mohammed Abdullah Alshawsh [b,*]

[a] Department of Pharmacology, School of Pharmaceutical Sciences, Universiti Sains Malaysia, Penang 11800, Malaysia
[b] Department of Pharmacology, Faculty of Medicine, Universiti Malaya, Kuala Lumpur 50603, Malaysia
[c] Department of Pharmacology, Faculty of Pharmacy, Arab International University (AIU), Damascus, Syria
[d] Division of Biomedical Sciences, School of Pharmacy, University of Nottingham Malaysia, Semenyih 43500, Malaysia
[e] College of Pharmacy, Al Ain University, Al Ain 64141, United Arab Emirates

ARTICLE INFO

Article history:
Received 17 May 2022
Accepted 3 September 2022
Available online 14 September 2022

Keywords:
Orthosiphon aristatus
Orthosiphon stamineus
Medicinal plant
Systems pharmacology
Non-alcoholic fatty liver disease
Cellular target
Pathway enrichment analysis
Protein–protein interaction
Molecular docking
Oxidative stress
Inflammation

ABSTRACT

Non-alcoholic fatty liver disease (NAFLD) is one of the most common complications of a metabolic syndrome caused by excessive accumulation of fat in the liver. *Orthosiphon stamineus* also known as *Orthosiphon aristatus* is a medicinal plant with possible potential beneficial effects on various metabolic disorders. This study aims to investigate the *in vitro* inhibitory effects of *O. stamineus* on hepatic fat accumulation and to further use the computational systems pharmacology approach to identify the pharmacokinetic properties of the bioactive compounds of *O. stamineus* and to predict their molecular mechanisms against NAFLD. Methods: The effects of an ethanolic extract of *O. stamineus* leaves on cytotoxicity, fat accumulation and antioxidant activity were assessed using HepG2 cells. The bioactive compounds of *O. stamineus* were identified using LC/MS and two bioinformatics databases, namely the Traditional Chinese Medicine Integrated Database (TCMID) and the Bioinformatics Analysis Tool for the Molecular Mechanism of Traditional Chinese Medicine (BATMAN-TCM). Pathway enrichment analysis was performed on the predicted targets of the bioactive compounds to provide a systematic overview of the molecular mechanism of action, while molecular docking was used to validate the predicted targets. Results: A total of 27 bioactive compounds corresponding to 50 potential NAFLD-related targets were identified. *O. stamineus* exerts its anti-NAFLD effects by modulating a variety of cellular processes, including oxidative stress, mitochondrial β-oxidation, inflammatory signalling pathways, insulin signalling, and fatty acid homeostasis pathways. *O. stamineus* is significantly targeting many oxidative stress regulators, including JNK, mammalian target of rapamycin (mTOR), NFKB1, PPAR, and AKT1. Molecular docking analysis confirmed the expected high affinity for the potential targets, while the *in vitro* assay indicates the ability of *O. stamineus* to inhibit hepatic fat accumulation. Conclusion: Using the computational systems pharmacology approach, the potentially beneficial effect of *O. stamineus* in NAFLD was indicated through the combination of multiple compounds, multiple targets, and multicellular components.

* Corresponding authors at: Department of Pharmacology, School of Pharmaceutical Sciences, Universiti Sains Malaysia, Penang 11800, Malaysia (R.H.A. Zarzour) & Department of Pharmacology, Faculty of Medicine, Universiti Malaya, Kuala Lumpur 50603, Malaysia (M.A. Alshawsh).
E-mail addresses: raghdaa@usm.my (R.H. Al Zarzour), alshaweshmam@um.edu.my, raghdaa@usm.my, alshaweshmam@um.edu.my (M.A. Alshawsh).

Peer review under responsibility of King Saud University.

ELSEVIER Production and hosting by Elsevier

1. Introduction

Non-alcoholic fatty liver disease (NAFLD) is a major growing worldwide health problem, affecting more than 25 % of people worldwide (Younossi, 2019). NAFLD is characterized by the accumulation of excessive hepatic fat (simple steatosis) that can further progress to non-alcoholic steatohepatitis (NASH) with or without fibrosis (Alshawsh et al., 2022). NAFLD may worsen clinical outcomes by progressing from simple steatosis to hepatocyte damage, liver inflammation, fibrosis, and cirrhosis (Forlano et al., 2022).

https://doi.org/10.1016/j.jsps.2022.09.001
1319-0164/

NAFLD is significantly associated with metabolic syndrome traits, including insulin resistance, abdominal overweight and hyperlipidaemia (Paschos and Paletas, 2009). Furthermore, the triggering and progression of NAFLD are according to a multi-hit theory, which is based on the linkage of multiple biological processes, including dysregulation of lipogenesis and lipolysis, oxidative stress, inflammation, insulin resistance, glucose intolerance, mitochondrial dysfunction, and apoptosis, among other factors (Buzzetti et al., 2016).

Increased cellular oxidative stress and reduced antioxidant capacity are associated with the inflammatory process (Chen et al., 2020). Inflammation, in which the immune response to harmful stimuli, initiates a cascade of chemicals mediated by pro-inflammatory cytokines. However, persistent inflammation contributes to epithelial dysplasia triggered by nitrogen and reactive oxygen species (ROS) (Cheng et al., 2021). In addition, ROS is produced by alternating mitochondria, and endoplasmic reticulum, specifically by affecting the β-oxidation process. Essentially, the elevated levels of ROS modulate lipid metabolism and insulin signalling. Therefore, oxidative stress and inflammation play a central role in the pathogenesis of NAFLD (Alshehade et al., 2022; Chen et al., 2020).

Presently, there is no effective treatment for NAFLD; only weight loss, reduced intake of fat and sugar and administration of probiotics are the current management options (Schuppan and Schattenberg, 2013). As a result, it is important to search for a potential agent to treat NAFLD and avoid the onset of the severe condition (Alshawsh et al., 2022). Naturopathy and herbal products are the main resources for the development of hepatoprotective drugs (Ali et al., 2018). *Orthosiphon stamineus* (Blume) Miq. *(Orthosiphon aristatus*) is traditionally used in Southeast Asia as an herbal tea to treat several disorders, including kidney disorders, gastrointestinal tract disorders, obesity, and diabetes (Ashraf et al., 2018).

Previous phytochemical studies on *O. stamineus* have reported that the leaves contain high levels of flavones, polyphenols, bioactive proteins, glycosides, essential oils, and large amounts of potassium (Saidan et al., 2015; Seyedan et al., 2017). Twenty phenolic compounds have been isolated, including nine lipophilic flavones, two flavanol glycosides, and nine caffeic acid derivatives. The leaves contain a high concentration of phenolic compounds. Therefore, rosmarinic acid (RA), 3-hydroxy-5,6,7,4-tetramethoxyflavone, sinensetin, and eupatorin were considered marker compounds for the standardization of different *O. stamineus* leaf extracts (Saidan et al., 2015; Seyedan et al., 2017).

Furthermore, *O. stamineus* has been shown to have pharmacological effects in rat models such as anti-inflammatory, antioxidant, and anti-angiogenesis properties (Alshawsh et al., 2012; Ashraf et al., 2018; Sahib et al., 2009). More importantly, *O. stamineus* showed a hepatoprotective effect in Sprague Dawley rats (Alshawsh et al., 2011; Seyedan et al., 2017). It was also observed that *O. stamineus* extract reduced the necrotic changes in the liver tissue and reduced serum levels of aspartate transaminase and alanine transaminase (Seyedan et al., 2017). The beneficial hepatic effect is believed to be due to its antioxidant effects and the ability to prevent the depletion of glutathione levels (Alshawsh et al., 2012; Ashraf et al., 2018).

Systems pharmacology is an emerging and novel approach based on bioinformatics and computational chemistry, which is used to predict the biological targets of small bioactive compounds or drugs. Biological networks are considered complex system that interacts rather than single transduction pathways. Such interactions are relevant when drugs act on multiple targets in the network (Danhof, 2016). Systems pharmacology is a promising approach for the next-generation drug discovery model, especially because it analyses multiple target regulations and seeks the cellular mechanism of action, in contrast to the traditional, time-consuming and costly approach (Liu et al., 2013). Hence, in this study, we used computational systems pharmacology approach, molecular docking, and *in vitro* assays to explore the bioactive compounds of *O. stamineus* and to predict, and elucidate the cellular targets and molecular mechanisms of action of *O. stamineus* against NAFLD.

2. Materials and Methods

2.1. Plant's extraction preparation

The fresh leaves of *O. stamineus* were collected from the botanical garden at the University of Malaya (UM) and then identified by the KLU Herbarium (code: KLU49065). The leaves were dried in an oven (40 °C) and ground to a coarse powder. Subsequently, 400 g of powdered *O. stamineus* leaves were extracted with 4 L of ethanol (100 %) (R&M Chemical, UK) at room temperature with occasional shaking for three days by the maceration method (Abubakar and Haque, 2020). The *O. stamineus* crude extract was filtered with Whatman Grade 1 filter paper and then concentrated with a vacuum rotary evaporator (Büchi-R-200, Switzerland).

2.2. In vitro fat accumulation assessment

2.2.1. Cell culture

HepG2 cells were obtained from ATCC, USA. After thawing, the cells were cultured in Eagle's minimal essential medium (EMEM: ATCC, Cat. 30–2003), 1X non-essential amino acids (SAFC, USA, Cat. M7145), penicillin–streptomycin solution (100 IU/mL and 100 μg/mL, respectively; ATCC, Cat. 30–2300), growth was at 37 °C in a humidified atmosphere of 5 % CO_2. At confluence, cells were trypsinized (0.05 % trypsin/0.53 mM EDTA).

2.2.2. Cytotoxicity assay

Cytotoxicity was assessed using the CCK-8 assay (MedChem Express, USA, Cat. HY-K0301) by utilising the highly water-soluble tetrazolium salt WST-8, which produces a water-soluble formazan dye (Zhang et al., 2020). HepG2 cells were seeded in triplicates at 4000 cells/well in 96-well plates with 100 μl of the medium in each well. The serial concentrations of *O. stamineus* crude extract (1000, 500, 250, 125, 62.5, 31.25, 15.6 μg/ml) were prepared in 1X PBS (Sigma-Aldrich, USA, Cat. P4417). Treatment was added after 12 h of seeding and carried out for three-time points (i.e., 24 h, 48 h, and 72 h). A fresh culture medium alone was used as a negative control. Then, each plate was incubated at 37 °C with 10 μl of CCK-8 solution for 2 h, and the absorbance was measured at 450 nm using a microplate reader (VersaMax, USA). Equation (1) was used to calculate the cell cytotoxicity percentage (CT%).

$$CT\% = \frac{C_{Abs} - S_{Abs}}{C_{Abs}} \times 100 \quad (1)$$

where C_{Abs} is the mean absorbance value of the negative control, and S_{Abs} is the mean absorbance value of the sample.

2.2.3. Detection of intracellular fat accumulation

At 50 % confluence, cells were exposed to a 1:2 mixture of palmitic acid (Sigma-Aldrich, USA, Cat. P0500) and oleic acid (Alfa Aesar, Cat. ALF 031997.06) conjugated to a BSA ratio of 1:5 (Pingitore et al., 2019). Post-steatotic, cells were exposed to the treatment for three-time points (i.e., 24 h, 48 h, and 72 h). The post-treatment medium was removed from each well and gently washed with 1x PBS. Then, a 100 μl Nile Red working solution (300 ng/mL Nile Red (Sigma, USA, Cat 19123) and 1 μg/mL Hoechst 33,342 (Sigma, USA, Cat B2261) in PBS was added and incubated at 37 °C with 5 % CO_2 for 15 min. Then, cells were washed with 1x PBS

and fat accumulated droplets were imaged directly with a fluorescence microscope with excitation and emission maxima of 488/550 nm for the Nile Red and 350/461 nm for Hoechst 33,342 (Greenspan et al., 1985).

2.2.4. The antioxidant activity of O. stamineus

Cells were seeded in a T-25 flask in uniform numbers, after reaching 50 % confluency, the cells were exposed to 0.5 mM FA for 24 h, then treated with filtered *O. stamineus* (53, 75, 150 μg/ml) for another 24 h. Then the cells were collected and lysed by 1 % SDS. The total protein content in each sample was quantified using the Bradford assay (Ernst and Zor, 2010). Lipid peroxidation was measured in the cell lysate by a thiobarbituric acid reaction (Ohkawa et al., 1979) using a malondialdehyde (MDA) colourimetric assay kit (Elabscience, China, Cat. E-BC-K025-S). In addition, the total superoxide dismutase (SOD) (Canvax Biotech, Spain, Cat. CA061) and glutathione peroxidase (GPx) (Elabscience, China, Cat. E-BC-K096-S) were measured with colourimetric assay kits. All the assays were performed according to the manufacturer's protocol.

2.3. Identifying the bioactive compounds of O. stamineus

2.3.1. LC/MS analysis

The analysis method was adapted from an earlier study (Saidan et al., 2015; Sawada and Hirai, 2013). Briefly, a filtered stock solution (1 mg/mL) of *O. stamineus* extract was prepared in methanol: water (1:1). The chromatographic separation was carried out using a C18 column and high-performance liquid chromatography device equipped with the Agilent 6500 series Q-TOF LC/MS system (Sawada and Hirai, 2013). The entire analysis time was 20 min at a flow rate of 1 mL/min.

2.3.2. Bioactive compounds screening libraries

The bioactive compounds of *O. stamineus* from different plant parts were screened using two libraries. The first was the Traditional Chinese Medicine Integrated Database (TCMID; http://bidd.group/TCMID/ access date: 30/06/2022), which is a unique systems pharmacology platform for Chinese herbal medicines that explores the relationships between drugs, targets, and diseases. The second was the Bioinformatics Analysis Tool For The Molecular Mechanism Of Traditional Chinese Medicine (BATMAN-TCM; http://bionet.ncpsb.org.cn/batman-tcm/) (Liu et al., 2016), which is the first online bioinformatics tool developed on the Internet, to study the molecular mechanisms of herbal medicine, and the search was conducted using the Chinese name of *O. stamineus* (Xiong Rui Zhuang Zhi Guan Cao).

2.3.3. Bioactive compounds filtration

The potential bioactive compounds of *O. stamineus* were filtered based on oral bioavailability score (OB $\geq$ 50 %) (Martin, 2005) and drug-likeness score (DL $\geq$ 0.18) (Hu et al., 2018). The Drug Likeness Score was determined using the Molsoft platform (https://molsoft.com/), which uses a machine learning model based on 5,000 marketed drugs from the World Drug Index (Positives) and 10,000 carefully selected non-drug compounds (Negatives) (Hu et al., 2018). SwissADME was used to investigate the physicochemical descriptors and predict pharmacokinetic properties, i.e., absorption, distribution, metabolism, and excretion (http://www.swissadme.ch) (Daina et al., 2017).

2.4. Toxicity

Predicting compound toxicities is an important part of the drug design development process. Toxic doses are often given as LD50 values in mg/kg body weight. The LD50 is the median lethal dose, which indicates the dose at which 50 % of test subjects die upon exposure to a compound. Toxicity classes are defined according to the globally harmonized system of classification and labelling of chemicals. In this study, we used ProTox-II (https://tox-new.charite.de/protox_II/) to estimate the toxicity of *O. stamineus* bioactive compounds using molecular similarity, fragment propensities, most frequent characteristics, and machine-learning (Banerjee et al., 2018). In addition, a decision tree approach model was used for the toxicity pathway, depicting the first key events in the adverse pathway. The tested substances are divided into six main classes, and these classes are further subdivided into a total of 25 subclasses. This model is mainly based on toxicity data from various *in vivo* models, which can provide a mechanistic understanding of empirical results and can help to strengthen risk assessment (Bauer et al., 2018). We used the iSafeRat® tool (https://www.isaferat.kreatis.eu/), which offers reliable *in silico* approaches with endpoint values equal to those obtained from experimental models, with reduced costs and time.

2.5. NAFLD-related genes

The genes associated with NAFLD were identified using the human disease database known as MalaCards (https://www.malacards.org; ID: FTT008 & NNL005), which is an integrated human disease database (Rappaport et al., 2017). In addition, the Kyoto Encyclopedia of Genes and Genomes (KEGG) disease database (Release 98.0; https://www.genome.jp/kegg/disease/) was also used to retrieve NAFLD-related genes (ID: H01333). KEGG is a database resource for understanding high-level functions of biological systems and the utility of molecular-level information, particularly large-scale molecular datasets generated by genome sequencing and other high-throughput experimental technologies (Kanehisa et al., 2017). Moreover, Online Mendelian Inheritance in Man (OMIM) database (https://www.omim.org/entry/613282) was also used to have a comprehensive search of the NAFLD-related genes.

2.6. Identifying the molecular targets of O. stamineus

Due to the diversity of *O. stamineus* compounds, the extract can target multiple proteins, making target identification a crucial step in understanding the molecular mechanism underlying the beneficial effects of *O. stamineus*. The 3D structures of the compounds were obtained from PubChem (https://pubchem.ncbi.nlm.nih.gov/). Prediction of the targets of the compounds was performed with BATMAN-TCM (Liu et al., 2016), which uses a similarity-based method to predict potential targets of bioactive plant compounds (Perlman et al., 2011). The score cut-off was chosen to be 20 and the adjusted *P*-value $\leq$ 0.05. Additionally, the Swiss target prediction platform (Daina et al., 2019) (http://www.swisstargetprediction.ch/) was used to predict the molecular targets, which uses computational predictions of bioactive molecular targets based on similarity to known ligands (Gfeller et al., 2013). The potential targets of the bioactive compounds to treat NAFLD were retrieved by matching the predicted target of each compound to the NAFLD-related gene list. The official symbols of the targets of *O. stamineus* compounds were retrieved from NCBI; https://www.ncbi.nlm.nih.gov/gene. In addition, to get an overview of the interaction between the potential targets and the bioactive compounds of *O. stamineus*, an interaction network was constructed with STRING (https://string-db.org/) (Szklarczyk et al., 2015), mapped with Cytoscape (V. 3.8.2) (Doncheva et al., 2019) and clustered by Markov clustering algorithm (Brohée and van Helden, 2006).

2.7. Pathway enrichment analysis

The associated molecular pathways of potential targets of *O. stamineus* were analysed using three bioinformatics databases to better understand the biological processes. Firstly, protein analysis through evolutionary relationships (PANTHER) (http://pantherdb.org/) was used to classify proteins (and their genes), which is typically used to aid in high-throughput analysis (Mi et al., 2019). Secondly, KEGG pathway enrichment was performed to study the biological effects of the *O. stamineus* compounds at the pathway level using DAVID (database for annotation, visualization, and integrated discovery; https://david.ncifcrf.gov/) (Huang et al., 2009). Lastly, the Reactome database (https://reactome.org/; release 76) was used to analyse the general targets of *O. stamineus* compounds (without matching with NAFLD-related genes). Reactome is an open-source, manually curated, and peer-reviewed pathway database (Jassal et al., 2020). A false discovery rate (FDR) $\leq$ 0.05 was selected, and the species was only limited to "Homo sapiens".

2.8. Molecular docking of bioactive compounds

The bioactive compounds of *O. stamineus* were docked to potential targets to confirm the interaction between the receptor and the ligand. The candidate compounds and the crystal structure of the

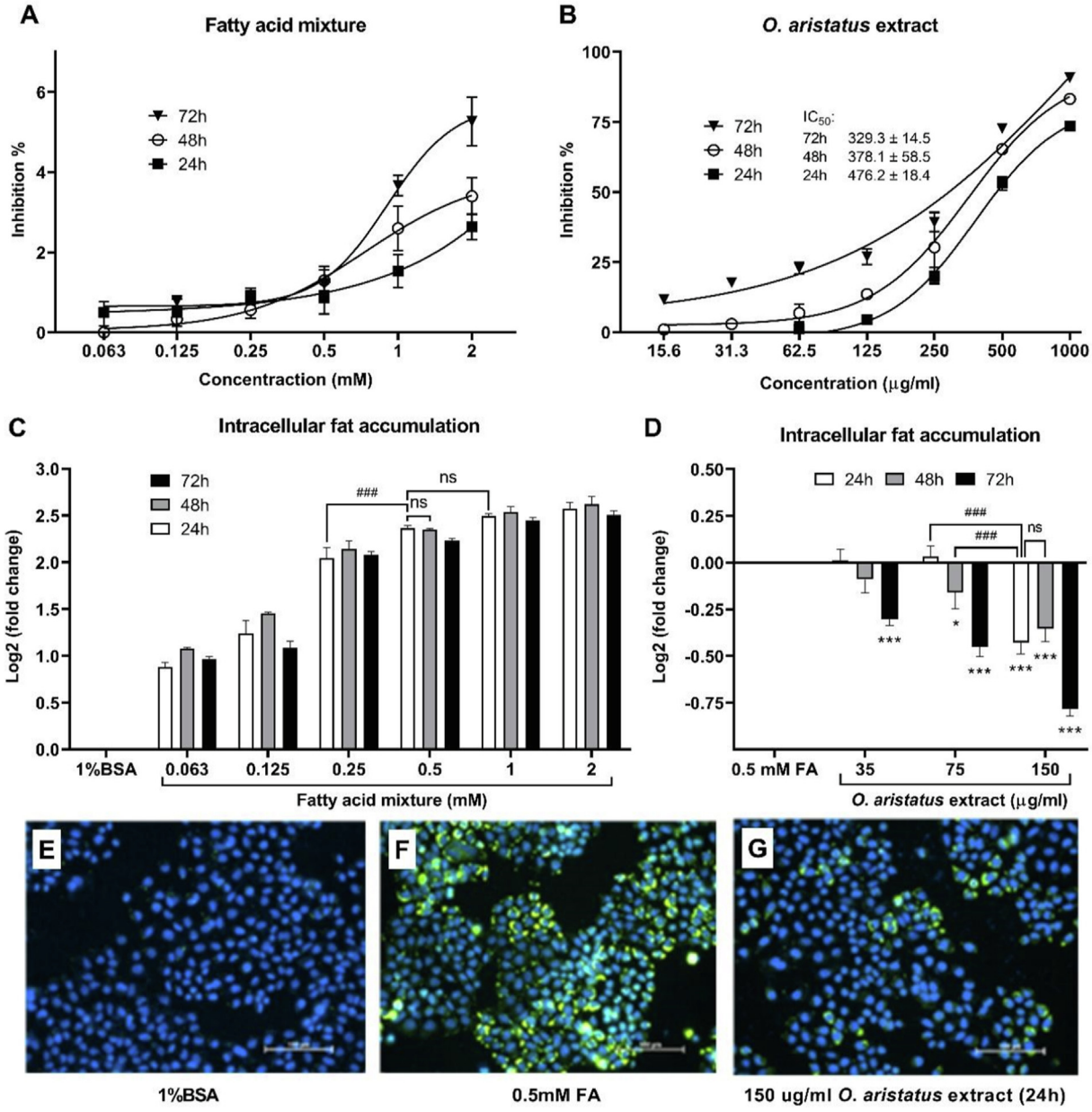

Fig. 1. Cytotoxicity and intracellular fat content of fatty acid mixture (FA) and *O. stamineus* extract at three-time points (24 h, 48 h, and 72 h). **A:** Cytotoxicity of palmitic acid and oleic acid mixture (1:2) against HepG2 cells expressed as inhibition of viability. **B**: Cytotoxicity of *O. stamineus* against HepG2 cells expressed as inhibition of viability. Concentration scales were logarithmised to obtain the relative response curves. Values were represented as mean ± SD, n = 3. **C**: Intracellular fat accumulation after treatment of the cells with different FA concentrations compared to the negative control (1 %BSA). The data were presented as mean ± SD, n = 3. ### $p \leq 0.001$. **D**: Intracellular fat accumulation after treating the cells with different concentrations of *O. stamineus* extract compared to the negative control (0.5 mM FA). (*) indicates the level of significance when compared to the negative control at the corresponding time point, and (#) indicates the level of significance when compared to the corresponding groups as indicated. The total fluorescence intensity of the Nile Red, as an indicator of the intracellular fat content, was normalized to the cell number and then compared to the corresponding negative control by calculating the log2 (fold change). Data were presented as mean ± SD, n = 3. * $p \leq 0.05$, *** $p \leq 0.001$, ### $p \leq 0.001$. **E, F, G**: Green colour is Nile Red stain (FITC filter), and blue colour is Hoechst 33,342 (DAPI filter) indicating nuclear counterstain.

target proteins were downloaded from the PubChem database and RCSB protein data bank (https://www.rcsb.org/) respectively, and then prepared with PyMOL (V. 2.4). Docking was done with Autodock Vina (V. 1.1.2) (Sharoen Y. M. Lim et al., 2022; Sharoen Yu Ming Lim et al., 2022; Trott and Olson, 2010). The water molecules have been removed, and the hydrogen atoms added. The exhaustiveness was set to 20, the number of modes was 50, and the energy range was 3.0 kcal/mol. Docking was performed blindly by adjusting the grid box based on the whole protein. The ligand bond was kept rotatable except for the double and triple bonds, and the energy was minimized by 5000 steps. Docking conformations with the lowest binding energy were selected and visualized using a Discovery Studio visualizer (V. 21.1).

2.9. Construction of the NAFLD pathway

An integrated "NAFLD pathway" was manually developed based on protein–protein interaction (PPI) network data to better understand the mechanisms underlying *O. stamineus*'s beneficial effects against NAFLD (Cui et al., 2021).

2.10. Statistical analysis

The *in vitro* data analysis was performed using the two-way ANOVA followed by Tukey's multiple comparisons test. GraphPad Prism version 8.0.2 for Windows (GraphPad Software, USA) was used to perform statistical analysis. The *Homo sapiens* was chosen for all the pathway enrichment analyses, which were performed using the annotated genes with Benjamini-Hochberg FDR as multiple test correction. *P*-values $\leq$ 0.05 were considered statistically significant.

3. Results

3.1. The in vitro results

3.1.1. Cytotoxicity and intracellular fat accumulation

As shown in Fig. 1A, the fatty acid mixture (FA) was relatively safe with<6 % inhibition of cells proliferation even after 72 h, while the IC_{50} of *O. stamineus* was 476.2 ± 18.4 μg/ml after 24 h of the treatment (Fig. 1B). After examining cytotoxicity, the intracellular fat accumulation was assessed over three-time points (24 h, 48 h, and 72 h). Various FA concentrations were used to determine the best concentration that effectively induces intracellular fat accumulation. As shown in Fig. 1C, 0.5 mM of FA significantly revealed a higher intracellular fat accumulation compared to 0.25 mM of FA, and there was no significant difference between 0.5 mM and 1 mM of FA after 24 h of fatty acid exposure (Fig. 1C). In addition, there was no significant difference between 24 and 48 h of 0.5 mM FA treatment. Hence, this concentration (0.5 mM) of FA was chosen to induce fat accumulation in HepG2 cells for 24 h, then the cells were treated with non-cytotoxic doses (35, 75, and 150 μg/ml) of *O. stamineus* extract (Fig. 1D). The highest dose (150 μg/ml) showed a significant reduction in intracellular fat accumulation at all tested time points when compared to the negative control (0.5 mM FA) at the same time point (Fig. 1D). Interestingly, the effect of reducing the intracellular fat accumulation by treating with 150 μg/ml *O. stamineus* extract for 24 h was significantly greater than the effect of the other two doses when compared at the same time point (Fig. 1D).

3.1.2. The antioxidant activities of O. stamineus

As shown in Fig. 2, the *O. stamineus* showed good antioxidant activity. Both GPx and SOD enzymes were increased significantly after treating the cells with medium and high concentrations (75 and 150 μg/ml, respectively). In addition, cells induced with 0.5 mM FA showed a significant increase in MDA compared to the non-induced cells (1 % BSA). Lipid peroxidation was alleviated by the high dose of *O. stamineus* (150 μg/ml) as indicated by the lower MDA levels; however, the difference compared to the untreated control (0.5 mM FA) was not significant.

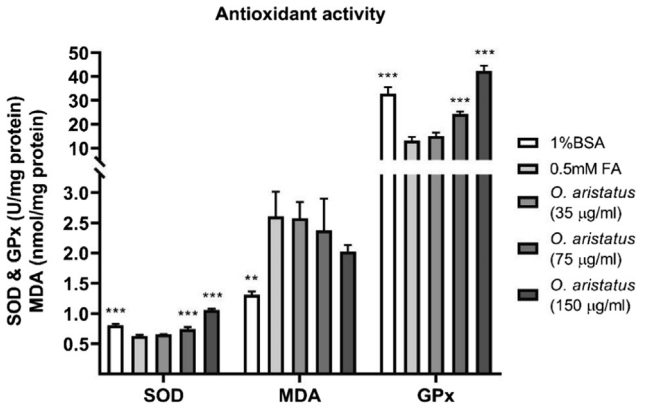

Fig. 2. The antioxidant and anti-lipid peroxidation activity of the *O. stamineus* extract in fatty acid-induced HepG2 cells. Intracellular fat accumulation was induced by treating cells with 0.5 mM fatty acid mixture (FA) for 24 h and then treating with different concentrations of *O. stamineus* (35, 75, and 150 μg/ml) for an additional 24 h. Data were presented as mean ± SD, n = 3, ** $p \leq 0.01$, and *** $p \leq 0.001$ compared to 0.5 mM FA control.

3.2. Identification of the bioactive compounds of O. stamineus

A total of 136 *O. stamineus* compounds were identified using LC/MS analysis of the ethanolic plant extract, online databases (TCMSP and BATMAN-TCM) and literature searches. Finally, after filtering the compounds based on OB $\geq$ 50 % and DL $\geq$ 0.18, a total of 27 compounds were found (Table 1) and considered to be bioactive compounds that are mainly responsible for the beneficial effects of *O. stamineus*.

The BOILED-EGG model (Daina and Zoete, 2016) is used to predict the most active compounds that could be passively absorbed by the gut. As shown in Fig. 3, about eight compounds can passively cross through the blood–brain barrier. However, some compounds (e.g., Cirsimaritin, No. 14) have been predicted to be effluated from the central nervous system through p-glycoprotein action.

3.3. Target identification and analysis

The human molecular targets for each bioactive compound were predicted using two different databases (BATMAN-TCM and Swiss Target Prediction Platform), and the *P*-value was set to be <0.05. Consequently, Gene Cards and OMIM databases were used to search for NAFLD-related genes. A total of 264 genes were obtained. A total of 50 potential targets of *O. stamineus* against NAFLD were identified by overlap, the significantly predicted targets of the bioactive compounds with the NAFLD-related genes. The interaction network between the potential targets and the bioactive compounds of *O. stamineus* is shown in Fig. 4.

3.4. Pathway analysis of the potential targets

The pathway enrichment analysis was performed using multiple database analyses to deepen molecular processes and the development of relationships between the potential targets of *O. stamineus* bioactive compounds.

Table 1
The properties of the filtered bioactive compounds of *O. stamineus*.

No.	Compound	LC/MS [3]				PubChem ID	DL [4]	OB [5]	Formula	iSafeRat [6]	Toxicity class [7]	LD_{50} [8]	References
		RT [1]	MW [2]	Ion Mode	Fragmentation pattern (*m*/*z*)								
1	3,7-Dimethyluric acid	3.01	196.06	+	74; 142; 161; 196; 198	91,611	0.37	55 %	C7H8N4O3	2.1 & p6.5	3	800	LC/MS
2	P-Coumaric Acid	4.22	164.16	–	93; 101; 119; 163	637,542	−0.81	85 %	C9H8O3	3.2	5	2850	(Ashraf et al., 2018)
3	Protocatechuic Acid	5.61	154.12	–	108; 110; 123; 153; 154	72	0.23	56 %	C7H6O4	5.2	4	2000	(Bakr et al., 2016)
4	N-(Hydrocinchonidin-8′-yl)-4-azido-2-hydroxybenzamide	6.85	598.12	+	59; 217; 327; 486; 574; 599	656,579	1.12	56 %	C26H27IN6O3	6.6	4	600	LC/MS
5	Hinokiflavone	7.12	538.09	+	270; 283; 335; 377; 403; 479; 539	5,281,627	0.66	55 %	C30H18O10	1.2	5	4000	LC/MS
6	Dipyrocetyl	7.95	238.05	+	43; 126; 154; 196; 238	68,093	0.38	56 %	C11H10O6	5.2	5	2021	LC/MS
7	Phylloflavan	9.11	498.15	+	68; 73; 129; 135; 175; 189; 319; 408; 497	457,885	1.26	55 %	C26H26O10	4.3 & 4.4	4	1000	LC/MS
8	Rosmarinic Acid	9.21	360.08	+	139; 159; 171; 197; 361	5,281,792	0.37	56 %	C18H16O8	3.2	5	5000	LC/MS, (Akowuah et al., 2004; Nishizawa et al., 1990; Sumaryono et al., 1991)
9	Disopyramide	9.55	339.23	+	72; 91; 114; 195; 239; 339	3114	0.72	55 %	C21H29N3O	1.2 & 5.2 / an6.2	3	343	LC/MS
10	Cryptotanshinone	9.55	296.36	+	51; 77; 105; 210	160,254	−0.16	85 %	C19H20O3	3.2 & 4.4	6	8000	LC/MS, (Liang et al., 2017)
11	Oxyayanin-B	9.72	360.08	+	121; 139; 233; 361	442,621	0.34	55 %	C18H16O8	4.3 & 4.4	5	5000	LC/MS
12	Pachypodol	10.26	344.09	–	270; 298; 313; 328; 343	5,281,677	0.28	55 %	C18H16O7	1.2 & m4.3	5	5000	LC/MS
13	Sinensetin	12.26	372.37	–	59; 136; 164; 262; 372	145,659	0.29	55 %	C20H20O7	1.1.	5	5000	LC/MS, (Akowuah et al., 2004; Guo et al., 2019; Malterud et al., 1989)
14	Cirsimaritin	12.79	314.29	+	167; 272; 285; 300; 315	188,323	0.47	55 %	C17H14O6	1.2 & m4.3	5	4000	LC/MS, (Guo et al., 2019)
15	Hydroxy-Octadecatrienoic Acid	14.47	294.43	–	177; 193; 203; 221; 236; 257; 275; 293	5,312,775	−0.51	85 %	C18H30O3	5.2	6	20,000	LC/MS, (Ji et al., 2017)
16	Propanoylagmatine	15.75	186.15	+	93; 137; 186; 209 (M + Na)+	439,760	0.42	55 %	C8H18N4O	2.1	4	700	LC/MS
17	Embelin	15.93	294.18	–	137; 150; 179; 294	3218	−0.02	85 %	C17H26O4	3.2 & 4.4	4	2000	LC/MS
18	5,7-Dihydroxyflavone 7-benzoate	16.25	358.08	+	135; 147; 153; 187; 211; 277; 258	5,575,368	0.35	55 %	C22H14O5	1.2	5	4000	LC/MS
19	3′-Hydroxy-5,6,7,4′-Tetramethoxyflavone	16.3	358.34	+	165; 284; 299; 342; 257	7,020,615	0.44	55 %	C19H18O7	1.2 & m4.3	5	4000	(Liu et al., 2017; Yam et al., 2007)
20	7,3′,4′-Tri-O-Methylluteolin	NA	328.32	NA	NA	5,272,653	0.23	55 %	C18H16O6	1.2	5	4000	(Tezuka et al., 2000)
21	Betulinic Acid	NA	456.70	NA	NA	64,971	0.25	85 %	C30H48O3	5.2	5	2610	(Ashraf et al., 2018)
22	Danshensu	NA	314.33	NA	NA	11,600,642	0.57	55 %	C18H18O5	3.2	5	4500	(Li et al., 2016; Liang et al., 2017; Zhou et al., 2011)
23	Dihydrotanshinone I	NA	278.30	NA	NA	11,425,923	−0.48	85 %	C18H14O3	3.2 & 4.4	6	8000	(Liang et al., 2017)
24	Eupatorin	NA	344.32	NA	NA	97,214	0.46	55 %	C18H16O7	1.2 & m4.3	5	4000	BATMAN-TCM, TCMID, (Akowuah et al., 2004; Malterud et al., 1989; Sumaryono et al., 1991; Zhou et al., 2011)
25	Ladanein	NA	572.64	NA	NA	3,084,066	0.41	55 %	C31H40O10	2.1	5	3700	BATMAN-TCM, TCMID, (Malterud et al., 1989; Zhou et al., 2011)
26	Salvigenin	NA	328.32	NA	NA	161,271	0.45	55 %	C18H16O6	1.2 & m4.3	5	4000	(Tezuka et al., 2000)

(*continued on next page*)

Table 1 (*continued*)

No.	Compound	LC/MS [3]				PubChem ID	DL [4]	OB [5]	Formula	iSafeRat [6]	Toxicity class [7]	LD_{50} [8]	References
		RT [1]	MW [2]	Ion Mode	Fragmentation pattern (*m/z*)								
27	Tanshinoldehyde	NA	310.34	NA	NA	124,268	−0.15	85 %	C19H18O4	3.2 & 4.4	6	8000	(Ji et al., 2017; Xie et al., 2017)

– iSafeRat mechanism of action classes:
Class (1.1) indicates non-polar narcosis for all species; class (1.2 & 5.2 / an6.2) indicates probable binding to ACh receptors (muscarinic or nicotinic) disrupting the normal nerve signal transmissions for animals & alkalinization of cells, corrosion if directly applied, for all species; class (1.2 & m4.3) indicates o-demethylation, then RedOx cycle between reduced and oxidized quinone for mammals. Polar narcosis for all species; class (1.2) indicates polar narcosis for all species; class (2.1 & p6.5) indicates blocking of electron transfer at the photosystem II > inhibits O_2 production for plants & hydrolytic pro-destabilisation for all species; class (2.1) indicates enzymatic hydrolysis to acid & alcohol/amine + narcosis of the parent compound, for all species; class (3.2 & 4.4) indicates soft electrophile reactivity and RedOx cycling for all species; class (3.2) indicates Michaël addition with proteins residues, generating adducts for all species; class (4.3 & 4.4) indicates oxidation by tyrosinase/CYP450 to quinone > protein & DNA adducts & RedOx cycling for all species; class (5.2) indicates release of protons in the cytosol of cells for all species; class (6.6) indicates binding at opioid receptors for animals.
– Toxicity classes:
Class (1) indicates fatal if swallowed ($LD_{50} \leq 5$ mg/kg); class (2) indicates fatal if swallowed ($5 < LD_{50} \leq 50$ mg/kg); class (3) indicates toxic if swallowed ($50 < LD_{50} \leq 300$ mg/kg); class (4) indicates harmful if swallowed ($300 < LD_{50} \leq 2000$ mg/kg); class (5) indicates may be harmful if swallowed ($2000 < LD_{50} \leq 5000$ mg/kg); class (6) indicates non-toxic ($LD_{50} > 5000$ mg/kg).
NA: Non-applicable.
[1] Retention Time (min).
[2] Molecular Weight (g/mol).
[3] The MS spectra can be found in the supplementary data (Table S1).
[4] Drug-likeness score (only compounds with DL ≥ 0.18 were included).
[5] Oral bioavailability score (only compounds with OB ≥ 50 % were included).
[6] iSafeRat mechanism of action class.
[7] Toxicity class.
[8] Lethal dose (mg/kg).

3.4.1. KEGG enrichment analysis

The pathways associated with *O. stamineus* in NAFLD treatment were elucidated by KEGG enrichment pathway analysis. The significantly enriched signalling pathways (FDR < 0.001) are shown in Table 2. These genes directly contributed to the progression of NAFLD and many related signalling pathways, including inflammation, insulin resistance, and the PPAR pathways.

3.4.2. Reactome analysis of potential targets

The potential targets were analysed using the Reactome platform. Multiple signalling pathways have been found to be associated with NAFLD, including fatty acid metabolism, lipid metabolism, insulin signalling and inflammation-related signalling pathways, such as the interleukins IL4 and IL13. Even more important is oxidative stress by significantly targeting key proteins such as cytochrome C (CYCS), glycogen synthase kinase-3 beta (GSK3B), interleukin 6 (IL6), mitogen-activated protein kinase-8 (MAPK8)/c-Jun *N*-terminal kinase (JNK1), mitogen-activated protein kinase-9 (MAPK9)/c-Jun *N*-terminal kinase (JNK2), mitogen-activated protein kinase-10 (MAPK10)/c-Jun *N*-terminal kinase (JNK3), mammalian target of rapamycin (MTOR), nuclear factor kappa B subunit 1 (NFKB1), v-rel avian reticuloendotheliosis viral oncogene homolog A (RELA), and sirtuin 1 (SIRT1). However, compared to the Reactome analysis of the total predicted targets, this is generally involved in the apoptosis and cell cycle-related signalling pathways. On the other hand, potential target pathways are more likely to cause metabolic disorders and cancer.

3.4.3. PANTHER analysis

The potential targets were also analysed using the PANTHER (Protein Analysis Through Evolutionary Relationships) database, which is based on bioinformatic algorithms developed to classify proteins (and their genes) to facilitate high-throughput analysis (Mi et al., 2013; Thomas et al., 2003). Fig. 5 shows the connections between a potential target and known signalling pathways investigated with PANTHER. A variety of signalling pathways related to NAFLD were significantly associated, including oxidative stress by affecting the proteins MAPK8 (JNK1), MAPK9 (JNK2), and MAPK10 (JNK3) and chemokine and cytokine-mediated inflammation by affecting C—C Motif Chemokine Ligand 2 (CCL2), inhibitor of kappa light polypeptide gene enhancer in B-cells, kinase beta (IKBKB), cyclooxygenase-2 (COX2), AKT Serine/Threonine Kinase 2 (AKT2), RELA, Phosphatidylinositol-4,5-Bisphosphate 3-Kinase Catalytic Subunit Alpha (PIK3CA), AKT Serine/Threonine Kinase 1 (AKT1), Nuclear Factor Kappa B Subunit 1 (NFKB1), IL6, and Interleukin-1 beta (IL1B). In addition, we found that angiogenesis, hypoxia, and insulin signalling pathways are significantly involved. Surprisingly, multiple pathways related to neurological diseases such as Parkinson's, Alzheimer's, and Huntington's have been implicated, possibly related to the agents that can cross the BBB. For example, dihydrotanshinone I was found to be able to cross the BBB by BOILED-EGG model and a recent study suggested using this compound to treat Alzheimer's disease as it was found to increase amyloid-β clearance and decrease Tau phosphorylation via autophagy enhancing involved with AMPK/mTOR pathway (Bao et al., 2020). Furthermore, dihydrotanshinone I alleviated the pathological damage caused by spinal cord injury and promoted the neuronal functional recovery (Yu and Qian, 2020). In addition, recent evidence has identified liver dysfunction as a new player in Alzheimer's progression (Estrada et al., 2019). An interesting point is the positive effect of the bioactive compounds on both diseases. However, this assumption has to be validated experimentally.

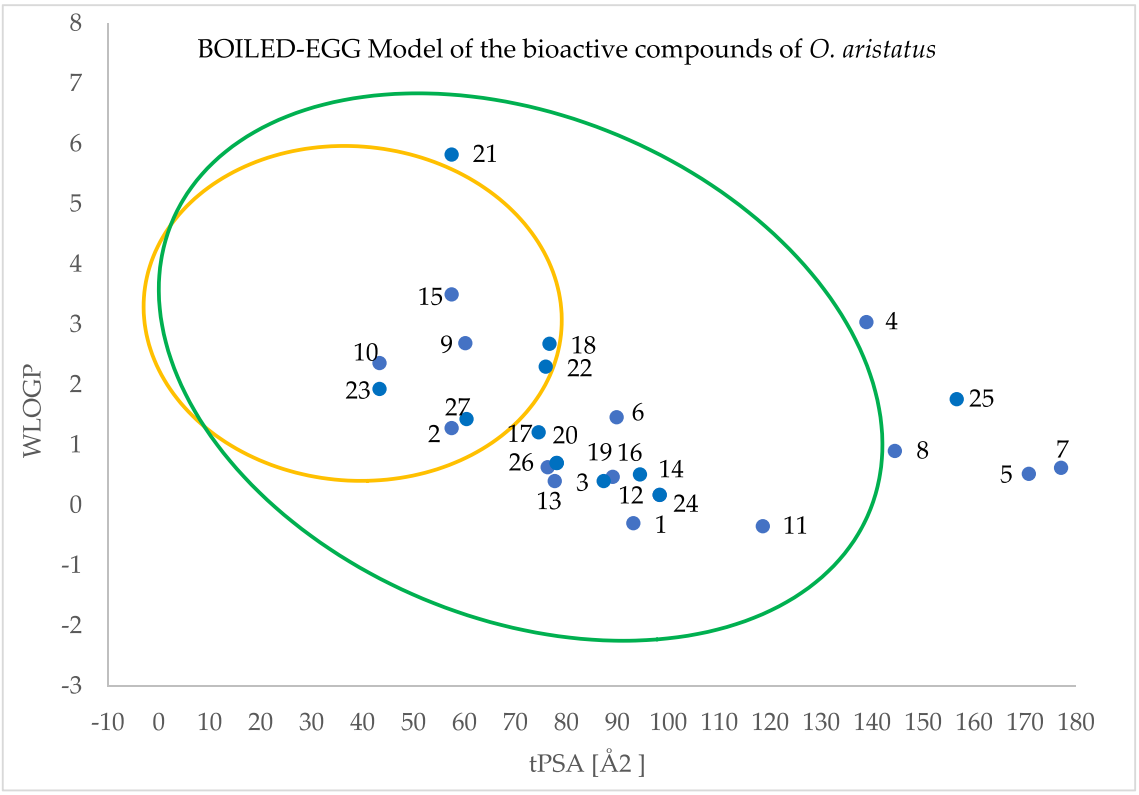

Fig. 3. The Boiled-Egg construction model. The compounds within the green area are predicted to be passively absorbed from the gastrointestinal tract. Compounds within the yellow area are predicted to passively cross the blood–brain barrier (e.g. dihydrotanshinone I). The compound number is given in Table 1.

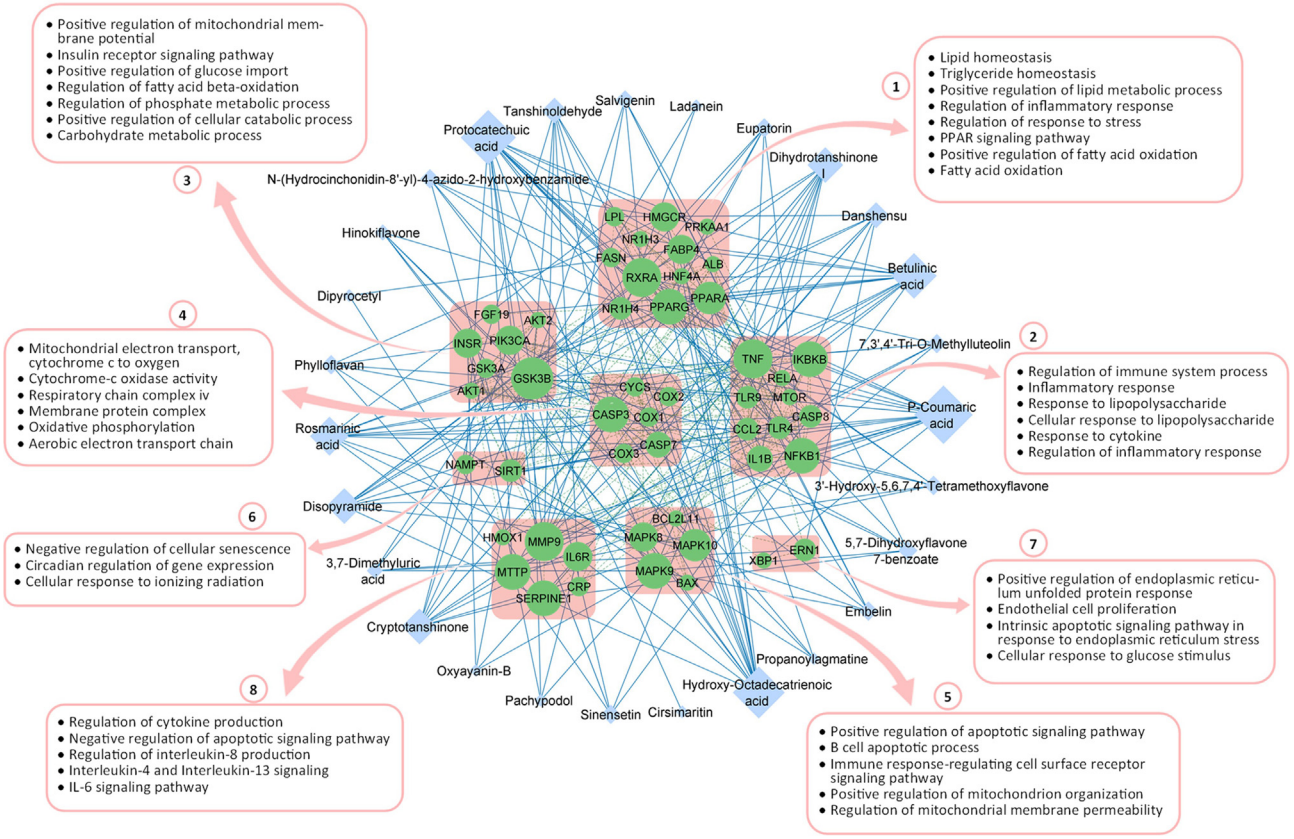

Fig. 4. Interaction network between proteins and bioactive compounds. The green ellipse nodes are the potential targets (n = 50) and the blue diamond nodes are the bioactive compounds of *O. stamineus* (n = 27). The blue edges represented the interactions between them (n = 410). The size of the nodes correlates with the number of interactions with the bioactive compounds. Proteins were clustered (1–8) using the Markov clustering algorithm (inflation value was 2.5). The biological process involved for each cluster was presented.

Table 2
Top significant pathways of KEGG enrichment analysis of the potential targets of O. stamineus.

Term name	Term ID	Adjusted p-value	-LOG$_{10}$(adjusted p-value)	T [1]	Q [2]	T ∩ Q [3]
Non-alcoholic fatty liver disease	KEGG:04932	2.026E−38	37.69	150	49	30
Lipid and atherosclerosis	KEGG:05417	1.688E−23	22.77	214	49	24
Alzheimer disease	KEGG:05010	5.894E−18	17.23	369	49	24
Chagas disease	KEGG:05142	1.412E−17	16.85	101	49	16
Insulin resistance	KEGG:04931	3.498E−17	16.46	108	49	16
Apoptosis	KEGG:04210	3.976E−17	16.40	136	49	17
TNF signalling pathway	KEGG:04668	4.374E−17	16.36	112	49	16
Adipocytokine signalling pathway	KEGG:04920	1.988E−15	14.70	69	49	13
Hepatitis B	KEGG:05161	1.157E−14	13.94	162	49	16
IL-17 signalling pathway	KEGG:04657	6.252E−14	13.20	92	49	13
Pathways in cancer	KEGG:05200	6.534E−14	13.18	529	49	23
Hepatitis C	KEGG:05160	1.287E−13	12.89	157	49	15
Diabetic cardiomyopathy	KEGG:05415	2.841E−13	12.55	203	49	16
Colorectal cancer	KEGG:05210	5.861E−13	12.23	86	49	12
Insulin signalling pathway	KEGG:04910	1.079E−10	9.97	137	49	12
MAPK signalling pathway	KEGG:04010	4.601E−08	7.34	294	49	13
Parkinson disease	KEGG:05012	5.983E−07	6.22	249	49	11
cAMP signalling pathway	KEGG:04024	1.190E−05	4.92	216	49	9
PPAR signalling pathway	KEGG:03320	1.277E−05	4.89	75	49	6
Hepatocellular carcinoma	KEGG:05225	1.198E−04	3.92	166	49	7

1: The total pathway protein 2: The quantity of tested proteins 3: the total involved tested proteins in the pathway.

3.4.4. Gene Ontology analysis

Further analysis using the Gene Ontology (GO) database describes the biological domain in terms of three aspects, namely, biological process, cellular component, and molecular function.

3.4.4.1. Biological process. The larger biological processes are accomplished through multiple molecular activities such as signal transduction or glucose transmembrane transport. Taking that a biological process is not equivalent to a pathway, as it represents the dynamics of multiple molecular activities that would describe a pathway. The potential founded targets involved in biological processes, such as lipids and fatty acids biosynthesis and homeostasis, as well as biological processes related to inflammation such as Nuclear Factor Kappa B (NF-κB) signalling (Table 3).

3.4.4.2. Cellular component. Unlike the other GO aspects, cellular component classes do not relate to processes but cellular anatomy. The major cellular components associated with the potential targets of *O. stamineus* are related to the mitochondria, justifying the involvement of the bioactive compounds in the oxidative stress and inflammatory pathways, as demonstrated earlier.

3.4.4.3. Molecular function. Molecular function describes activities at the molecular level, such as "catalysis" or "transport," while the GO molecular function term represents activities rather than the entities (molecules or complexes) that perform the actions and does not specify where, when, or in what context the action occurs. These actions are described from two distinct but related points of view: (1) biochemical activity and (2) a role as a component in a larger system/process. The results can be found in the, the potential targets of *O. stamineus* mostly function via threonine/serine kinase activity, which is a family of enzymes that play a role in the regulation of cell proliferation, programmed cell death (apoptosis), cell differentiation and energy homeostasis (Nuñez-Durán et al., 2018).

3.5. Molecular docking

Molecular docking was used to assess and validate the interactions between the *O. stamineus*' bioactive compounds and the potential targets. A total of nine bioactive compounds were selected based on the degree of interaction, including 3′-hydrox y-5,6,7,4′-tetramethoxyflavone, 7,3′,4′-tri-o-methylluteolin, betulinic acid, cirsimaritin, danshensu, eupatorin, rosmarinic acid, salvigenin, and sinensetin. Ten potential targets of the selected bioactive compounds have been implicated in NAFLD, including glycogen synthase kinase-3 beta (GSK3B), lipoprotein lipase (LPL), matrix metalloproteinase-9 (MMP9), microsomal triglyceride transfer protein (MTTP), NF-κB1, PIK3, peroxisome proliferator-activated receptor alpha (PPARA), peroxisome proliferator- activated receptor gamma (PPARG), retinoid X receptor alpha (RXRA), and tumor necrosis factor (TNF). The proteins targeted by only one compound were excluded since the anti-NAFLD activity is thought to result mainly from hitting multiple targets. The binding affinity of the ligand–protein complex was evaluated (Table 4). Binding energy less than −6 was recognized as high affinity.

In addition, the inhibition constant (Ki) was calculated, which reflects the binding affinity of the inhibitor and provides an indication for future research on this compound. The smaller the Ki, the higher the binding affinity (Bachmann and Lewis, 2005). For example, all the compounds targeting glycogen synthase kinase-3 beta (GSK3B) had a good affinity, but cirsimaritin had the lowest Ki values, outperforming the other compounds. Also, the nuclear factor kappa B subunit 1 (NF-κB1) ligands have almost the same affinity, but the Ki constant signifies the good competitor. However, three of them had almost similar values (≈17 μM); in this case, we believe that the best competitor is the one that has the highest concentration in the administered *O. stamineus* extract. The conformations with the highest affinity are shown in Fig. 6.

4. Discussion

Orthosiphon stamineus, commonly known as Java tea, is a popular herbal plant grown in East Asia. Its extract is traditionally used to improve several disorders, as it shows anti-inflammatory, analgesic, hypoglycaemic, hypolipidemic, and anti-obesity effects (Ashraf et al., 2018; Seyedan et al., 2017). Due to the high phenol content of *O. stamineus*, including lipophilic flavones (e.g., sinensetin, 3′-hydroxy-5,6,7,4′-tetramethoxyflavone, and eupatorin), glycosides (e.g., orthosiphonin), and caffeic acid derivatives (e.g., rosmarinic acid), there is a rising interest in studying the benefits of *O. stamineus* (Ashraf et al., 2018). Consequently, it is strongly believed that *O. stamineus* has pharmacological effects in the treatment of one of the main complications of metabolic syndrome, i.e.,

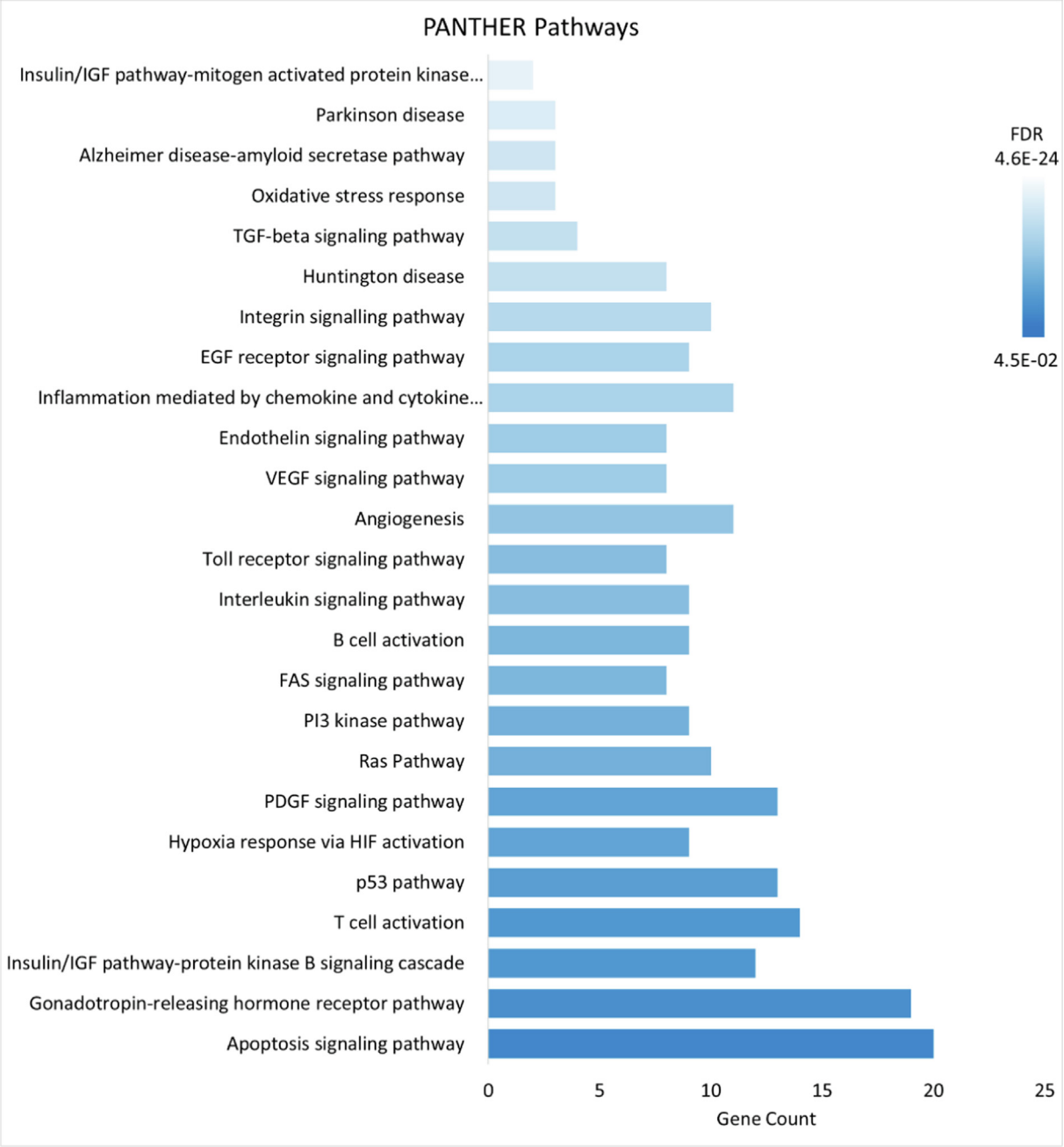

Fig. 5. The top 25 pathways of the PANTHER analysis of the potential targets of *O. stamineus*.

NAFLD. In this study, we used emerging computational systems pharmacology to predict and explore the effects and molecular mechanisms of and investigate how the bioactive compounds of the *O. stamineus* could improve NAFLD progression, which could facilitate the development of novel therapies and may improve responses to currently available therapies.

Computational systems pharmacology is an emerging approach that is widely used to predict and illustrate the mechanism of action, pharmacological activity, and protein–protein/RNA interaction network (Gao et al., 2020; Sookoian et al., 2020). Therefore, this approach provides a novel, time, and cost-saving method. This study is one of the first to use a systems pharmacology approach to investigate the beneficial effects and cellular mechanisms of action of *O. stamineus* against NAFLD.

The *in vitro* assays showed a significant reduction in the intracellular fat accumulation after treatment with *O. stamineus* extract in HepG2 cells. Although in this study the characterization of the HepG2 cells was not carried out, previous studies revealed that the *in vitro* fatty acid-induced HepG2 mimics steatosis and has a similar pattern of molecular mechanism as NAFLD (Müller and Sturla, 2019). Several studies showed that fatty acid-induced HepG2 is dose-dependent characterized by increased expression of sterol regulatory element-binding transcription factor 1, CD36, diacylglycerol transferase 2, and other genes involved in *de novo* lipogenesis. In addition, the intracellular fat accumulation induces the production of tumour necrosis factor-alpha, and other pro-inflammatory cytokines (Cui et al., 2010; Müller and Sturla, 2019; Su et al., 2019). Also, the reduction of intracellular fat by

Table 3
The top biological processes that related to the potential targets of O. stamineus.

Term name	Term ID	Adjusted p-value	-LOG$_{10}$(adjusted p-value)	T [1]	Q [2]	T ∩ Q [3]
Cellular response to chemical stimulus	GO:0070887	2.646E−22	21.58	3443	50	44
Response to oxygen-containing compound	GO:1901700	2.105E−21	20.68	1748	50	35
Response to chemical	GO:0042221	7.474E−21	20.13	4829	50	47
Positive regulation of metabolic process	GO:0009893	8.140E−21	20.09	3873	50	44
Cell death	GO:0008219	4.464E−19	18.35	2306	50	36
Response to organic substance	GO:0010033	5.722E−19	18.24	3457	50	41
Apoptotic process	GO:0006915	8.065E−19	18.09	1998	50	34
Positive regulation of macromolecule metabolic process	GO:0010604	1.380E−18	17.86	3568	50	41
Positive regulation of cellular metabolic process	GO:0031325	1.784E−18	17.75	3342	50	40
Programmed cell death	GO:0012501	6.730E−18	17.17	2158	50	34
Cellular response to organonitrogen compound	GO:0071417	9.522E−18	17.02	671	50	23
Regulation of cell death	GO:0010941	2.795E−17	16.55	1740	50	31
Positive regulation of nitrogen compound metabolic process	GO:0051173	3.288E−17	16.48	3143	50	38
Negative regulation of apoptotic process	GO:0043066	3.319E−17	16.48	928	50	25
Negative regulation of programmed cell death	GO:0043069	5.159E−17	16.29	952	50	25
Regulation of protein metabolic process	GO:0051246	4.850E−15	14.31	2759	50	34
Response to hormone	GO:0009725	7.989E−15	14.10	958	50	23
Cellular response to chemical stress	GO:0062197	3.759E−14	13.42	356	50	16
Cellular response to lipid	GO:0071396	9.061E−13	12.04	617	50	18
Lipid localization	GO:0010876	2.440E−12	11.61	464	50	16

[1] The total pathway protein.
[2] The quantity of tested proteins.
[3] The total involved tested proteins in the pathway.

Table 4
Molecular docking of the selected bioactive compounds of *O. stamineus* and NAFLD targets.

No.	PDB ID	Protein Symbol	Ligand	Affinity (kcal/mol)	Ki (μM)	Number of H-Bonds
1.	5HLN	GSK3B	Eupatorin	−8.34	0.86	3
			3′-Hydroxy-5,6,7,4′-Tetramethoxyflavone	−7.52	3.45	4
			7,3′,4′-Tri-O-Methylluteolin	−8.31	0.80	2
			Cirsimaritin	−8.81	0.33	4
			Sinensetin	−7.29	4.49	2
			Salvigenin	−8.04	1.27	3
2.	6WN4	LPL	Danshensu	−6.51	16.73	2
			Rosmarinic Acid	−7.57	2.78	9
3.	1GKC	MMP9	Eupatorin	−8.48	0.59	6
			Danshensu	−7.57	2.79	5
			Rosmarinic Acid	−9.41	0.12	6
			3′-Hydroxy-5,6,7,4′-Tetramethoxyflavone	−8.11	1.14	7
4.	6I7S	MTTP	Eupatorin	7.81	1.89	9
			Rosmarinic Acid	−8.30	0.82	7
			3′-Hydroxy-5,6,7,4′-Tetramethoxyflavone	−7.70	2.23	7
			7,3′,4′-Tri-O-Methylluteolin	−7.57	2.81	7
			Cirsimaritin	−8.06	1.22	6
			Sinensetin	−7.42	3.60	6
			Salvigenin	−7.71	2.19	6
5.	1svc	NF-κB1	Eupatorin	−6.48	17.72	4
			3′-Hydroxy-5,6,7,4′-Tetramethoxyflavone	−6.29	24.14	3
			7,3′,4′-Tri-O-Methylluteolin	−6.39	20.67	4
			Cirsimaritin	−6.48	17.72	4
			Sinensetin	−5.82	53.53	5
			Salvigenin	−6.51	17.07	5
6.	4WWP	PIK3	Danshensu	−6.81	10.28	5
			3′-Hydroxy-5,6,7,4′-Tetramethoxyflavone	−7.601	2.68	8
			7,3′,4′-Tri-O-Methylluteolin	−8.27	0.85	6
			Cirsimaritin	−8.01	1.35	4
			Sinensetin	−7.61	2.62	8
7.	2REW	PPARA	Danshensu	−6.58	14.81	2
			Rosmarinic Acid	−8.88	0.30	4
8.	3ADS	PPARG	Danshensu	−6.24	26.39	3
			Rosmarinic Acid	−7.73	2.13	6
9.	2ZY0	RXRA	Eupatorin	−7.35	4.038	2
			3′-Hydroxy-5,6,7,4′-Tetramethoxyflavone	7.04	6.83	2
			7,3′,4′-Tri-O-Methylluteolin	−7.46	3.36	1
			Cirsimaritin	−7.82	1.83	1
			Salvigenin	−7.12	6.01	1
10.	4TWT	TNF	Eupatorin	−7.43	3.57	4
			Danshensu	−6.21	28.27	4
			Rosmarinic Acid	−6.66	13.11	3
			3′-Hydroxy-5,6,7,4′-Tetramethoxyflavone	−7.13	5.92	6
			7,3′,4′-Tri-O-Methylluteolin	−6.54	15.96	2
			Cirsimaritin	−6.51	16.64	4
			Sinensetin	−6.32	23.18	2
			Salvigenin	−6.45	18.52	0

PDB ID: Protein Data Bank ID (https://www.rcsb.org/); Ki: inhibitor constant.

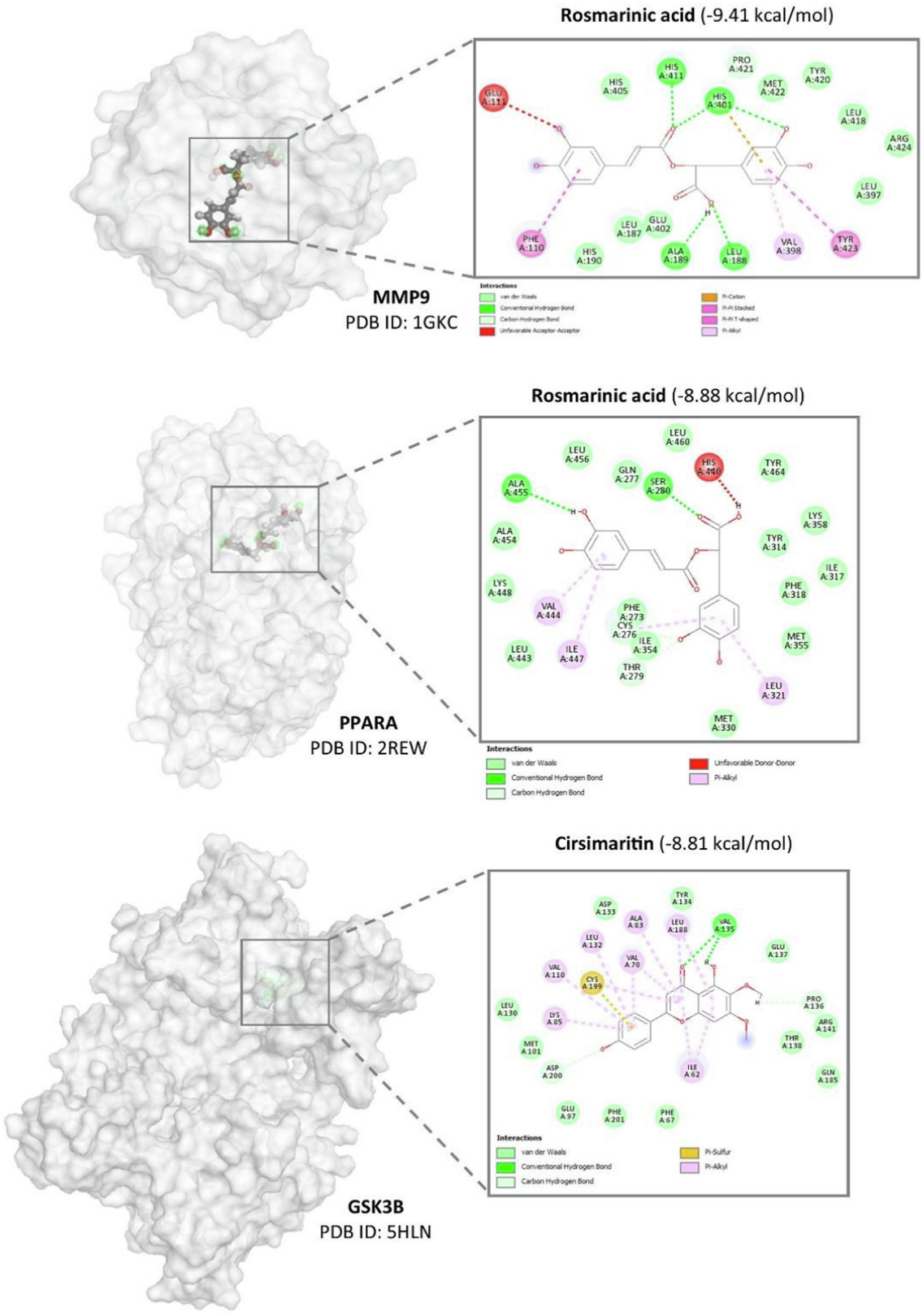

Fig. 6. Top three ligand-targets confirmation that had the highest affinity.

O. stamineus is aligned with antioxidant activity, specifically, the GPx and SOD enzymes activity.

As liver damage is associated with an increase in tissue lipid peroxidation as MDA and a decrease in tissue glutathione levels that are caused by oxidative stress (Ali et al., 2018), the antioxidant properties of *O. stamineus* have been proposed as a mechanism of the hepatoprotective properties of *O. stamineus* (Alshawsh et al., 2011). Furthermore, the reduction in the intracellular fat

accumulation by *O. stamineus* can be contributed to affecting fatty acid biosynthesis drives lipogenesis associated phenotypes such as increased lipid droplets accumulation and hepatocyte hypertrophy (Smith et al., 2020). Essentially, the final step in fatty acid biosynthesis is regulated by fatty acid synthase (FASN) catalysts and is believed to be a major determinant of hepatic fatty acids production by *de novo* lipogenesis (Dorn et al., 2010). Furthermore, cluster 1 of the targeted protein (Fig. 4) revealed that FASN and the other co-expressed proteins regulate lipid hemostasis, and this cluster is targeted by 19 bioactive compounds, suggesting an important role of *O. stamineus* in the regulation of lipid hemostasis. Based on previous studies, fatty acid-induced steatosis in cells was associated with fat accumulation and hypertrophy (Cetrullo et al., 2020). Since the results of our *in vitro* study showed that *O. stamineus* inhibits intracellular fat accumulation in HepG2 cells, this would be reflected in a reduction in hepatocyte hypertrophy.

The composition of *O. stamineus* was identified using LC/MS analysis combined with various databases, as well as assessed of its pharmacokinetic properties (e.g., absorption, lipophilicity, bioavailability, and toxicity). About two-thirds (n = 96) of the compounds were predicted to be absorbed from the gastrointestinal tract, and seven of them had a highly oral bioavailability rate (85 %). The molecular descriptors of the identified compounds were done according to different theoretical rules of medicinal chemistry (Lipinski, Ghose, Veber, Egan and Muegge). We have found that 18 compounds did not violate any of the DL rules, indicating a high ability to be biologically active.

The majority of the compounds were relatively safe, having a toxicity class of 5, indicating a low probability of being harmful if swallowed (Banerjee et al., 2018). The biochemical properties of bioactive compounds predict promised pharmacological effects in the human body, and are considered lead substances for the development and design of new drugs. The targets of the bioactive compounds and the NAFLD-related genes were identified through a combination of bioinformatics-based platforms. Potential targets were mainly involved in inflammatory and oxidative phosphorylation pathways and functions, mainly in the mitochondria. Based on these data, we propose that anti-NAFLD activity might be mediated through antioxidant and anti-inflammatory activities.

A total of 136 compounds of *O. stamineus* were identified in the present study. 27 bioactive compounds were filtered out, with 50 predicted potential targets related to NAFLD (Fig. 4). The regulation of these proteins is mainly responsible for the beneficial anti-NAFLD effects of *O. stamineus*, which rely on a multi-targeting effect. As shown in Fig. 4, multiple bioactive compounds were found to target the same protein, and the size of the illustrated targets (node) is correlated with the number of targeted bioactive compounds. For example, the microsomal triglyceride transfer protein (MTTP) is targeted by seven compounds, 18 compounds target glycogen synthase kinase-3 beta (GSK3B), and 6 compounds target peroxisome proliferator-activated receptor alpha (PPARA). Also, compounds like p-coumaric acid can target 18 proteins, and 12 proteins are hit by rosmarinic acid. These valuable data indicate that the bioactive compounds of *O. stamineus* could synergistically affect multiple proteins, besides justifying the traditional use of the plant to treat multiple diseases.

The network interactions revealed that acetyl-co A carboxylase alpha (ACACA) is targeted by 14-deoxo-14-o-acetylorthosiphol Y, and orthosiphol Y. ACACA is a cytosolic enzyme that catalyses the carboxylation of acetyl-CoA to malonyl-CoA, the first and rate-limiting step of *de novo* fatty acid biosynthesis (Colbert et al., 2010). ACACA has been identified as a key hub node with the highest connecting degree in NAFLD development (Liu et al., 2020).

Interestingly, network interactions revealed that PPARG and TNF are regulated by eight and nine bioactive compounds, respectively. It was reposted that PPARG and TNF as being associated with NAFLD development (Alshawsh et al., 2022; Alshehade et al., 2022). When the nuclear receptor, PPAR, is activated, it modulates the transcription of its target genes, such as acyl-CoA oxidase, alleviating hepatic steatosis by increasing fatty acid β-oxidation (Ables, 2012). In addition, activation of pro-inflammatory cytokines such as TNF, in adipose and liver tissues is implicated in playing an important role in NAFLD pathogenesis. Also, higher TNF serum levels were correlated with insulin resistance in NASH patients compared to patients with simple steatosis (Abiru et al., 2006).

NF-κB is a transcription factor that is the endpoint of a series of signal transduction events initiated by several biological processes, including inflammation, immunity, cell growth, and apoptosis (Beg and Baldwin, 1994). NF-κB is a homo- or heterodimeric complex formed by the rel-like domain-containing proteins, including RELA and NF-κB1, which are shown to be regulated by p-coumaric acid and seven compounds, respectively. NF-κB is controlled by various mechanisms of post-translational modification and subcellular compartmentalization as well as by interactions with other cofactors or corepressors. NF-κB complexes are held in the cytoplasm in an inactive state complexed with the NF-κB inhibitor, including IKBKB (inhibitor of nuclear factor-kappa B kinase subunit beta), which is hit by six compounds.

In a conventional activation pathway, I-kappa-B is phosphorylated by I-kappa-B kinases (IKKs) in response to different activators and subsequently degraded, thus liberating the active NF-κB complex translocation to the nucleus (Luedde and Schwabe, 2011). It was found that inhibiting the nuclear transcriptional activity of NF-κB will suppress inflammatory responses and prevent NAFLD's development and progression into NASH (Sun et al., 2021). NF-κB1 has important regulatory functions in inflammatory responses by acting as transcriptional activators promoting memory *T*-cell activation and regulating pro-inflammatory genes (e.g., TNF, and CCL2) expression in activated hepatic stellate cells (Locatelli et al., 2013). In relation, we have found that CCL2 is targeted by dihydrotanshinone I and tanshinoldehyde, indicating that the beneficial effects of *O. stamineus* result from targeting many targets in the inflammation pathways.

A previous experimental study confirmed the anti-inflammatory effects of eupatorin and sinensetin present in *O. stamineus* by suppressing the expression of the inflammatory genes, including iNOS, COX2 and TNF, and the production of inflammatory mediators such as nitric oxide (NO) (Laavola et al., 2012). Furthermore, the molecular docking analysis confirmed the good affinity of the bioactive compounds, which validated the target prediction method and confirmed the effectiveness of targeting NAFLD-related proteins.

To understand the cellular pathways involved in the pharmacological anti-NAFLD effects of *O. stamineus*, we used several well-known platforms to perform pathway enrichment analysis. Based on KEGG enrichment analysis, the top signalling pathways mainly focused on different kinase activities (mitogen-activated protein kinase (MAPK), PI3K-Akt, insulin, and AMP-activated protein kinase (AMPK) signalling pathways). Protein kinases (PKs), one of the largest protein families, play a crucial role in the pathophysiology of metabolic disorders, including NAFLD (Alshehade et al., 2022). PKs activate various intracellular signals by covalently binding phosphate to the side chains of serine, threonine, or tyrosine of the substrate proteins and can induce *gluco-* lipo-neogenesis, inflammation, cell differentiation, and apoptosis (Alshehade et al., 2022; Jiménez-Castro et al., 2019). In addition, KEGG analysis revealed the involvement of insulin-related signalling pathways (insulin resistance, type I, and type II diabetes mellitus). Inflammation-related pathways were also one of the dominant ones, i.e. NF-κB, mTOR, Toll-like receptors and TNF signalling pathways.

In addition, the Panther pathway analysis provides additional information over KEGG, such as involving the oxidative stress signalling pathway and apoptosis signalling pathways, which are both important in the progression of NAFLD. NAFLD is believed to be developed by the multiple-hit theory, assuming that liver damage is triggered by multiple factors, including oxidative stress-induced mitochondrial dysfunction, endoplasmic reticulum stress, endotoxin-induced, and inflammatory cytokines, among many others (Alshehade et al., 2022; Buzzetti et al., 2016). In addition, the Panther analysis showed that 11 genes are associated with angiogenesis, in which the formation of new blood vessels from pre-existing ones is an important pathophysiological mechanism contributing to the progression of NAFLD. Many factors that trigger NAFLD include tissue hypoxia (Lefere et al., 2020), which is also regulated by *O. stamineus* by targeting the HIF activation pathway. Therefore, it is not surprising that *O. stamineus* can exert anti-NAFLD effects through multiple signalling pathways. Further analysis using the GO database was also performed, the biological process analysis showed trends consistent with KEGG and Panther analysis. The disruption of lipid metabolic balance in the liver is not only directly related to lipid metabolism, lipopolysaccharide-mediated signalling pathway and lipid biosynthesis process, but also with inflammation, and oxidative stress (Pei et al., 2020).

Previous studies showed a reduction in the serum levels of triglyceride, total cholesterol, and low-density lipoprotein in mice fed a high-fat diet and orally administered with *O. stamineus* extract and rosmarinic acid (Sahib et al., 2009). Furthermore, the main cellular components targeted by *O. stamineus* are the mitochondria, which support anti-oxidant and anti-inflammatory activities as the main pharmacological activities.

Furthermore, the general mechanistic mind map (Fig. 7) revealed the multifactorial contribution of *O. stamineus* bioactive compounds against NAFDL progression through regulation of many signalling pathways. In particular, the improvement in

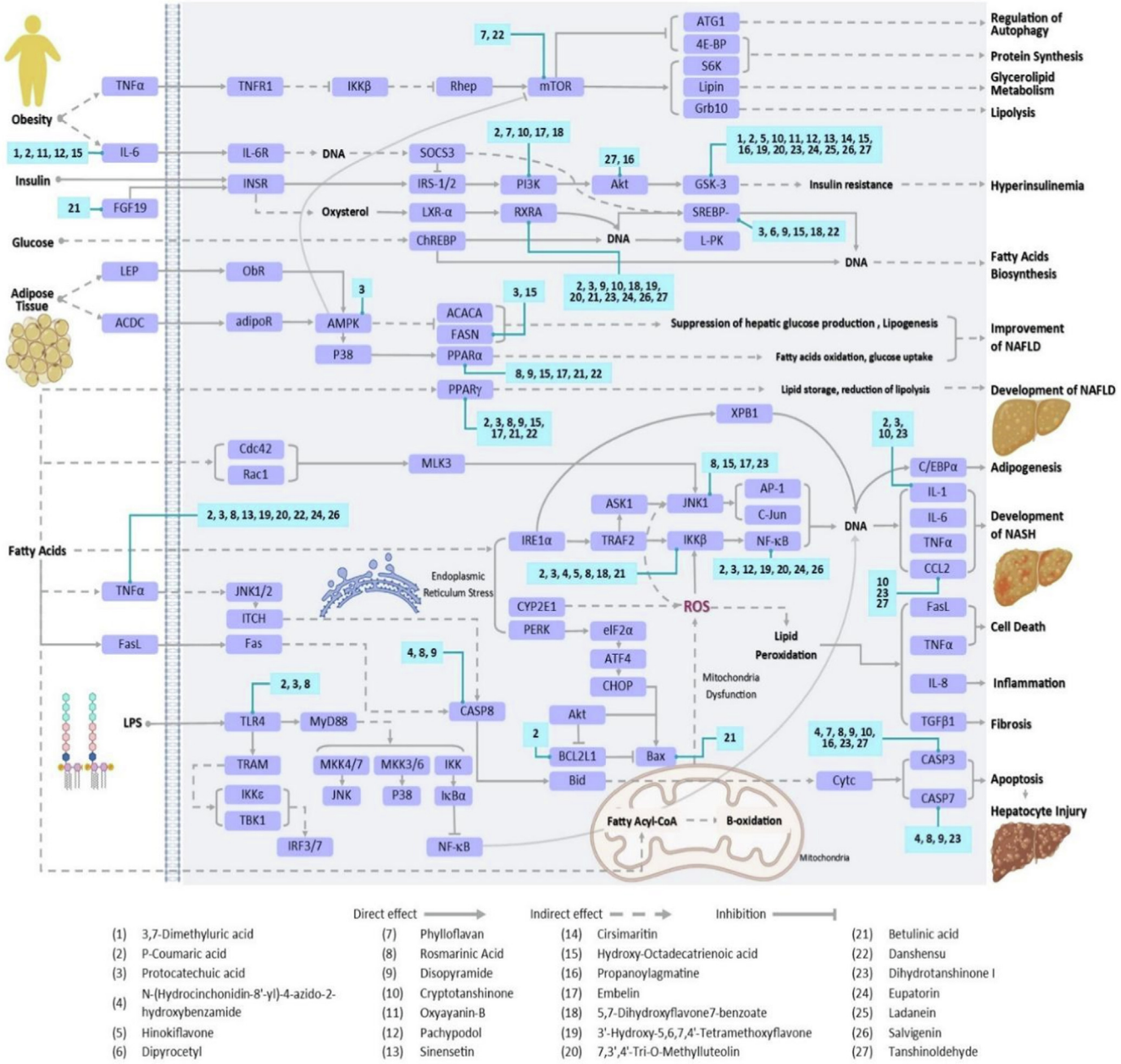

Fig. 7. Mind map of the molecular mechanism of action of *O. stamineus* in improving NAFLD.

hepatic insulin resistance in adipose tissue and liver through the regulation of AKT and GSK3 nodes was supported by a previous study showing that *O. stamineus* possessed significant antidiabetic activity by attenuating glucose-6-phosphate dehydrogenase, glycogen storage, and glucose-6-phosphatase activity (Koteswara Rao et al., 2014). In addition, the regulation of many signalling pathways, including oxidative stress, and inflammation, has been widely implicated in ameliorating NAFLD and preventing its progression to the advanced stage, i.e., NASH. TNFα is regulated at both the upstream and downstream levels, as well as NF-κB, toll-like receptor 4 (TLR4), and Caspase-3,-7,-8, which is supported by a recent study published in Neoplasia that found rosmarinic acid, the main compound of *O. stamineus*, attenuates the expression of anti-apoptotic factors, by modulating TLR4, NF-κB and STAT3 activation (Jin et al., 2021). Furthermore, enhancing NAFLD contributes to the regulation of PPAR, AMPK, ACACA and FASN.

This study is limited by the nature of the *in silico* molecular docking, as it predicts the bioactive compounds that exert their effects by binding to specific targets and provides evidence of binding conformation, pattern, and affinity, but the directions of interaction (inhibition/stimulation) need to be confirmed using an appropriate animal or cell line models, particularly, as there are many factors influencing the final beneficial/adverse effects. For example, the variation of the concentrations of the compounds in the extract, the possibility of competitive binding interaction, antagonistic/additive/synergistic effects between the compounds and negative regulatory pathways. However, a well-designed study is needed to examine the mechanism of the compounds alone and in combination.

5. Conclusions

The systems pharmacology approach was used in this study to identify the bioactive compounds of *O. stamineus* (n = 27) and to predict their potential targets (n = 50) involved in the progression of NAFLD. *O. stamineus*' compounds were relatively safe. Network analysis indicated that the *O. stamineus* might exert anti-NAFLD effects by regulating key proteins, such as JNK, AKT1, FASN, IKBKB, IL1A, MTOR, NF-κB1, PPARA, PPARG, PRKAA1, TLR4 and TNF. The analysis of the enrichment pathways of the potential targets using several databases (i.e., KEGG, Reactome, Panther, Go) revealed that the *O. stamineus* pharmacological activity derives from the regulation of various cellular pathways, including oxidative stress (JNK and NF-κB1), protein kinase activity (e.g., PI3K-AKT and AMPK), insulin signalling, PPAR signalling, fatty acid metabolism, and inflammation-related signalling pathways, such as interleukin signalling. Overall, this study provides a successful and novel approach to systematically predict the beneficial effects and the molecular mechanism of action of *O. stamineus* against NAFLD. In addition, the *in vitro* assay demonstrated a reduction in the intracellular fat accumulation after treatment with *O. stamineus* extract in HepG2 cells. From these results, it is concluded that *O. stamineus* offers good beneficial effects to improve NAFLD by containing multi-target compounds with antioxidant and anti-inflammatory activities. This research is the first step towards a more profound understanding of the molecular mechanism of action of this medicinal plant. Despite the success demonstrated, the main limitation relates to the computational nature of this study; therefore, follow-up mechanistic experimental investigations are necessary.

Funding

This research was funded by a research grant from the Universiti Malaya, Malaysia, project number (ST070-2021), a grant (No. 304/PFARMASI/6315201) provided by the School of Pharmaceutical Sciences, Universiti Sains Malaysia, and by the Ministry of Higher Education Malaysia Fundamental Research Grant Scheme (project code FRGS/1/2021/SKK0/USM/02/27).

Data Availability Statement:

The data that support the findings of the interaction network is available in the NDEx-The Network Data Exchange repository at https://doi.org/10.18119/N9330R.

Declaration of Competing Interest

The authors declare that they have no known competing financial interests or personal relationships that could have appeared to influence the work reported in this paper.

References

Abiru, S., Migita, K., Maeda, Y., Daikoku, M., Ito, M., Ohata, K., Nagaoka, S., Matsumoto, T., Takii, Y., Kusumoto, K., Nakamura, M., Komori, A., Yano, K., Yatsuhashi, H., Eguchi, K., Ishibashi, H., 2006. Serum cytokine and soluble cytokine receptor levels in patients with non-alcoholic steatohepatitis. Liver Int. 26, 39–45. https://doi.org/10.1111/j.1478-3231.2005.01191.x.

Ables, G.P., 2012. Update on Pparγ and nonalcoholic fatty liver disease. PPAR Res. 2012, 1–5. https://doi.org/10.1155/2012/912351.

Abubakar, A.R., Haque, M., 2020. Preparation of medicinal plants: Basic extraction and fractionation procedures for experimental purposes. J. Pharm. Bioallied Sci. 12, 1–10. https://doi.org/10.4103/jpbs.JPBS_175_19.

Akowuah, G.A., Zhari, I., Norhayati, I., Sadikun, A., Khamsah, S.M., 2004. Sinensetin, eupatorin, 3′-hydroxy-5, 6, 7, 4 ′-tetramethoxyflavone and rosmarinic acid contents and antioxidative effect of Orthosiphon stamineus from Malaysia. Food Chem. 87, 559–566. https://doi.org/10.1016/j.foodchem.2004.01.008.

Ali, M., Khan, T., Fatima, K., Ali, Q.u.A., Ovais, M., Khalil, A.T., Ullah, I., Raza, A., Shinwari, Z.K., Idrees, M., 2018. Selected hepatoprotective herbal medicines: Evidence from ethnomedicinal applications, animal models, and possible mechanism of actions. Phyther. Res. 32 (2), 199–215. https://doi.org/10.1002/ptr.5957.

Alshawsh, M.A., Abdulla, M.A., Ismail, S., Amin, Z.A., 2011. Hepatoprotective effects of Orthosiphon stamineus extract on thioacetamide-induced liver cirrhosis in rats. Evidence-based Complement. Altern. Med. 2011, 1–6. https://doi.org/10.1155/2011/103039.

Alshawsh, M.A., Abdulla, M.A., Ismail, S., Amin, Z.A., Qader, S.W., Hadi, H.A., Harmal, N.S., 2012. Free radical scavenging, antimicrobial and immunomodulatory activities of Orthosiphon stamineus. Molecules 17, 5385–5395. https://doi.org/10.3390/molecules17055385.

Alshawsh, M.A., Alsalahi, A., Alshehade, S.A., Saghir, S.A.M., Ahmeda, A.F., Zarzour, R.H.A., Mahmoud, A.M., 2022. A Comparison of the Gene Expression Profiles of Non-Alcoholic Fatty Liver Disease between Animal Models of a High-Fat Diet and Methionine-Choline-Deficient Diet. Molecules 27, 858. https://doi.org/10.3390/molecules27030858.

Alshehade, S., Alshawsh, M.A., Murugaiyah, V., Asif, M., Alshehade, O., Almoustafa, H., Al Zarzour, R.H., 2022. The role of protein kinases as key drivers of metabolic dysfunction-associated fatty liver disease progression: New insights and future directions. Life Sci. 305, 120732. https://doi.org/10.1016/j.lfs.2022.120732.

Ashraf, K., Sultan, S., Adam, A., 2018. Orthosiphon stamineus Benth. is an outstanding food medicine: Review of phytochemical and pharmacological activities. J. Pharm. Bioallied Sci. 10, 109–118. https://doi.org/10.4103/JPBS.JPBS_253_17.

Bachmann, K.A., Lewis, J.D., 2005. Predicting inhibitory drug-drug interactions and evaluating drug interaction reports using inhibition constants. Ann. Pharmacother. 39, 1064–1072. https://doi.org/10.1345/aph.1E508.

Bakr, R.O., Mohamed, S.A.E.H., Ayoub, N., 2016. Phenolic profile of centaurea aegyptiaca L. Growing in Egypt and its cytotoxic and antiviral activities. African J. Tradit. Complement. Altern. Med. 13, 135–143. https://doi.org/10.21010/ajtcam.v13i6.19.

Banerjee, P., Eckert, A.O., Schrey, A.K., Preissner, R., 2018. ProTox-II: A webserver for the prediction of toxicity of chemicals. Nucleic Acids Res. 46, W257–W263. https://doi.org/10.1093/nar/gky318.

Bao, Z., Zhang, H., Jiao, H., Chu, X., Fu, J., Wang, L., 2020. Dihydrotanshinone i Increase Amyloid-β Clearance and Decrease Tau Phosphorylation via Enhancing Autophagy. Pharmacology 105, 311–319. https://doi.org/10.1159/000503792.

Bauer, F.J., Thomas, P.C., Fouchard, S.Y., Neunlist, S.J.M., 2018. High-accuracy prediction of mechanisms of action using structural alerts. Comput. Toxicol. 7, 36–45. https://doi.org/10.1016/j.comtox.2018.06.004.

Beg, A.A., Baldwin, A.S., 1994. Activation of multiple NF-κB/Rel DNA-binding complexes by tumor necrosis factor. Oncogene 9, 1487–1492.

Brohée, S., van Helden, J., 2006. Evaluation of clustering algorithms for protein-protein interaction networks. BMC Bioinformatics 7, 488. https://doi.org/10.1186/1471-2105-7-488.

Buzzetti, E., Pinzani, M., Tsochatzis, E.A., 2016. The multiple-hit pathogenesis of non-alcoholic fatty liver disease (NAFLD). Metabolism 65, 1038–1048. https://doi.org/10.1016/j.metabol.2015.12.012.
Cetrullo, S., D'Adamo, S., Panichi, V., Borzì, R.M., Pignatti, C., Flamigni, F., 2020. Modulation of Fatty Acid-Related Genes in the Response of H9c2 Cardiac Cells to Palmitate and n-3 Polyunsaturated Fatty Acids. Cells 9, 537. https://doi.org/10.3390/cells9030537.
Chen, Z., Tian, R., She, Z., Cai, J., Li, H., 2020. Role of oxidative stress in the pathogenesis of nonalcoholic fatty liver disease. Free Radic. Biol. Med. 152, 116–141. https://doi.org/10.1016/j.freeradbiomed.2020.02.025.
Cheng, K.J., Mejia Mohammed, E.H., Khong, T.L., Mohd Zain, S., Thavagnanam, S., Ibrahim, Z.A., 2021. IL-1α and colorectal cancer pathogenesis: Enthralling candidate for anti-cancer therapy. Crit. Rev. Oncol. Hematol. 163,. https://doi.org/10.1016/j.critrevonc.2021.103398 103398.
Colbert, C.L., Kim, C.W., Moon, Y.A., Henry, L., Palnitkar, M., McKean, W.B., Fitzgerald, K., Deisenhofer, J., Horton, J.D., Kwon, H.J., 2010. Crystal structure of Spot 14, a modulator of fatty acid synthesis. Proc. Natl. Acad. Sci. U. S. A. 107, 18820–18825. https://doi.org/10.1073/pnas.1012736107.
Cui, W., Chen, S.L., Hu, K.Q., 2010. Quantification and mechanisms of oleic acid-induced steatosis in HepG2 cells. Am. J. Transl. Res. 2, 95–104.
Cui, Y., Ji, J., Hou, J., Tan, Y., Han, X., 2021. Identification of key candidate genes involved in the progression of idiopathic pulmonary fibrosis. Molecules 26, 1123. https://doi.org/10.3390/molecules26041123.
Daina, A., Michielin, O., Zoete, V., 2017. SwissADME: a free web tool to evaluate pharmacokinetics, drug-likeness and medicinal chemistry friendliness of small molecules. Sci. Rep. 7, 42717. https://doi.org/10.1038/srep42717.
Daina, A., Michielin, O., Zoete, V., 2019. SwissTargetPrediction: updated data and new features for efficient prediction of protein targets of small molecules. Nucleic Acids Res. 47, W357–W364. https://doi.org/10.1093/nar/gkz382.
Daina, A., Zoete, V., 2016. A BOILED-Egg To Predict Gastrointestinal Absorption and Brain Penetration of Small Molecules. ChemMedChem 11, 1117–1121. https://doi.org/10.1002/cmdc.201600182.
Danhof, M., 2016. Systems pharmacology – Towards the modeling of network interactions. Eur. J. Pharm. Sci. 94, 4–14. https://doi.org/10.1016/j.ejps.2016.04.027.
Doncheva, N.T., Morris, J.H., Gorodkin, J., Jensen, L.J., 2019. Cytoscape StringApp: Network Analysis and Visualization of Proteomics Data. J. Proteome Res. 18, 623–632. https://doi.org/10.1021/acs.jproteome.8b00702.
Dorn, C., Riener, M.O., Kirovski, G., Saugspier, M., Steib, K., Weiss, T.S., Gäbele, E., Kristiansen, G., Hartmann, A., Hellerbrand, C., 2010. Expression of fatty acid synthase in nonalcoholic fatty liver disease. Int. J. Clin. Exp. Pathol. 3, 505–514.
Ernst, O., Zor, T., 2010. Linearization of the Bradford protein assay. J. Vis. Exp. https://doi.org/10.3791/1918.
Estrada, L.D., Ahumada, P., Cabrera, D., Arab, J.P., 2019. Liver Dysfunction as a Novel Player in Alzheimer's Progression: Looking Outside the Brain. Front. Aging Neurosci. 11. https://doi.org/10.3389/fnagi.2019.00174.
Forlano, R., Mullish, B.H., Roberts, L.A., Thursz, M.R., Manousou, P., 2022. The Intestinal Barrier and Its Dysfunction in Patients with Metabolic Diseases and Non-Alcoholic Fatty Liver Disease. Int. J. Mol. Sci. 23, 662. https://doi.org/10.3390/ijms23020662.
Gao, S.-S., Sun, J.-J., Wang, X., Hu, Y.-Y., Feng, Q., Gou, X.-J., Rotenberg, S.A., 2020. Research on the Mechanism of Qushi Huayu Decoction in the Intervention of Nonalcoholic Fatty Liver Disease Based on Network Pharmacology and Molecular Docking Technology. Biomed. Res. Int. 2020, 1–12.
Gfeller, D., Michielin, O., Zoete, V., 2013. Shaping the interaction landscape of bioactive molecules. Bioinformatics 29, 3073–3079. https://doi.org/10.1093/bioinformatics/btt540.
Greenspan, P., Mayer, E.P., Fowler, S.D., 1985. Nile red: A selective fluorescent stain for intracellular lipid droplets. J. Cell Biol. 100, 965–973. https://doi.org/10.1083/jcb.100.3.965.
Guo, Z., Liang, X., Xie, Y., 2019. Qualitative and quantitative analysis on the chemical constituents in Orthosiphon stamineus Benth. using ultra high-performance liquid chromatography coupled with electrospray ionization tandem mass spectrometry. J. Pharm. Biomed. Anal. 164, 135–147. https://doi.org/10.1016/j.jpba.2018.10.023.
Hu, Q., Feng, M., Lai, L., Pei, J., 2018. Prediction of Drug-Likeness Using Deep Autoencoder Neural Networks. Front. Genet. 9. https://doi.org/10.3389/fgene.2018.00585.
Huang, D.W., Sherman, B.T., Lempicki, R.A., 2009. Systematic and integrative analysis of large gene lists using DAVID bioinformatics resources. Nat. Protoc. 4, 44–57. https://doi.org/10.1038/nprot.2008.211.
Jassal, B., Matthews, L., Viteri, G., Gong, C., Lorente, P., Fabregat, A., Sidiropoulos, K., Cook, J., Gillespie, M., Haw, R., Loney, F., May, B., Milacic, M., Rothfels, K., Sevilla, C., Shamovsky, V., Shorser, S., Varusai, T., Weiser, J., Wu, G., Stein, L., Hermjakob, H., D'Eustachio, P., 2020. The reactome pathway knowledgebase. Nucleic Acids Res. 48, D498–D503. https://doi.org/10.1093/nar/gkz1031.
Ji, D.e., Huang, Z.-Y., Fei, C.-H., Xue, W.-W., Lu, T.-L., 2017. Comprehensive profiling and characterization of chemical constituents of rhizome of Anemarrhena asphodeloides Bge. J. Chromatogr. B Anal. Technol. Biomed. Life Sci. 1060, 355–366.
Jiménez-Castro, C.-P., Gracia-Sancho, C.-R., Peralta, 2019. Mitogen Activated Protein Kinases in Steatotic and Non-Steatotic Livers Submitted to Ischemia-Reperfusion. Int. J. Mol. Sci. 20, 1785. https://doi.org/10.3390/ijms20071785.
Jin, B.R., Chung, K.S., Hwang, S., Hwang, S.N., Rhee, K.J., Lee, M., An, H.J., 2021. Rosmarinic acid represses colitis-associated colon cancer: A pivotal involvement of the TLR4-mediated NF-κB-STAT3 axis. Neoplasia (United States) 23, 561–573. https://doi.org/10.1016/j.neo.2021.05.002.
Kanehisa, M., Furumichi, M., Tanabe, M., Sato, Y., Morishima, K., 2017. KEGG: New perspectives on genomes, pathways, diseases and drugs. Nucleic Acids Res. 45, D353–D361. https://doi.org/10.1093/nar/gkw1092.
Koteswara Rao, N., Bethala, K., Patro Sisinthy, S., Sharmila Rajeswari, K., 2014. Antidiabetic activity of Orthosiphon stamineus benth roots in streptozotocin induced type 2 diabetic rats. Asian J. Pharm. Clin. Res. 7, 149–153.
Laavola, M., Nieminen, R., Yam, M., Sadikun, A., Asmawi, M., Basir, R., Welling, J., Vapaatalo, H., Korhonen, R., Moilanen, E., 2012. Flavonoids eupatorin and sinensetin present in Orthosiphon stamineus leaves inhibit inflammatory gene expression and STAT1 activation. Planta Med. 78, 779–786. https://doi.org/10.1055/s-0031-1298458.
Lefere, S., Devisscher, L., Geerts, A., 2020. Angiogenesis in the progression of non-alcoholic fatty liver disease. Acta Gastroenterol. Belg. 83, 301–307.
Li, Q., He, Y.N., Shi, X.W., Kang, L.Y., Niu, L.Y., Wang, X.G., Feng, W., 2016. Clerodens E-J, antibacterial caffeic acid derivatives from the aerial part of Clerodendranthus spicatus. Fitoterapia 114, 110–114. https://doi.org/10.1016/j.fitote.2016.08.021.
Liang, W., Chen, W., Wu, L., Li, S., Qi, Q., Cui, Y., Liang, L., Ye, T., Zhang, L., McPhee, D. J., 2017. Quality evaluation and chemical markers screening of salvia miltiorrhiza Bge. (Danshen) Based on HPLC Fingerprints and HPLC-MSn Coupled With Chemometrics. Molecules 22. https://doi.org/10.3390/molecules22030478.
Lim, S.Y.M., Loo, J.S.E., Alshagga, M., Alshawsh, M.A., Ong, C.E., Pan, Y., 2022a. Protein-Ligand Identification and In Vitro Inhibitory Effects of Cathine on 11 Major Human Drug Metabolizing Cytochrome P450s. Int. J. Toxicol. 41 (5), 355–366. https://doi.org/10.1177/10915818221103790.
Lim, S.Y.M., Loo, J.S.E., Alshagga, M., Alshawsh, M.A., Ong, C.E., Pan, Y., 2022b. In vitro and In silico studies of interactions of cathinone with human recombinant cytochrome P450 CYP(1A2), CYP2A6, CYP2B6, CYP2C8, CYP2C19, CYP2E1, CYP2J2, and CYP3A5. Toxicol. Reports 9, 759–768. https://doi.org/10.1016/j.toxrep.2022.03.040.
Liu, Z., Guo, F., Wang, Y., Li, C., Zhang, X., Li, H., Diao, L., Gu, J., Wang, W., Li, D., He, F., 2016. BATMAN-TCM: A Bioinformatics Analysis Tool for Molecular mechANism of Traditional Chinese Medicine. Sci. Rep. 6, 21146. https://doi.org/10.1038/srep21146.
Liu, J., Lin, B., Chen, Z., Deng, M., Wang, Y., Wang, J., Chen, L., Zhang, Z., Xiao, X., Chen, C., Song, Y., 2020. Identification of key pathways and genes in nonalcoholic fatty liver disease using bioinformatics analysis. Arch. Med. Sci. 16, 374–385. https://doi.org/10.5114/aoms.2020.93343.
Liu, H., Wang, J., Zhou, W., Wang, Y., Yang, L., 2013. Systems approaches and polypharmacology for drug discovery from herbal medicines: An example using licorice. J. Ethnopharmacol. 146, 773–793. https://doi.org/10.1016/j.jep.2013.02.004.
Liu, G.-D., Zhao, Y.-W., Li, Y.-J., Wang, X.-J., Si, H.-H., Huang, W.-Z., Wang, Z.-Z., Ma, S.-P., Xiao, W., 2017. Qualitative and quantitative analysis of major constituents from Dazhu Hongjingtian capsule by UPLC/Q-TOF-MS/MS combined with UPLC/QQQ-MS/MS. Biomed. Chromatogr. 31 (6), e3887. https://doi.org/10.1002/bmc.3887.
Locatelli, I., Sutti, S., Vacchiano, M., Bozzola, C., Albano, E., 2013. NF-κB1 deficiency stimulates the progression of non-alcoholic steatohepatitis (NASH) in mice by promoting NKT-cell-mediated responses. Clin. Sci. 124, 279–287. https://doi.org/10.1042/CS20120289.
Luedde, T., Schwabe, R.F., 2011. NF-κB in the liver-linking injury, fibrosis and hepatocellular carcinoma. Nat. Rev. Gastroenterol. Hepatol. 8, 108–118. https://doi.org/10.1038/nrgastro.2010.213.
Malterud, K.E., Hanche-Olsen, I.M., Smith-Kielland, I., 1989. Flavonoids from Orthosiphon spicatus. Planta Med. 55, 569–570. https://doi.org/10.1055/s-2006-962099.
Martin, Y.C., 2005. A bioavailability score. J. Med. Chem. 48, 3164–3170. https://doi.org/10.1021/jm0492002.
Mi, H., Muruganujan, A., Thomas, P.D., 2013. PANTHER in 2013: Modeling the evolution of gene function, and other gene attributes, in the context of phylogenetic trees. Nucleic Acids Res. 41, D377–D386. https://doi.org/10.1093/nar/gks1118.
Mi, H., Muruganujan, A., Ebert, D., Huang, X., Thomas, P.D., 2019. PANTHER version 14: more genomes, a new PANTHER GO-slim and improvements in enrichment analysis tools. Nucleic Acids Res. 47, D419–D426. https://doi.org/10.1093/nar/gky1038.
Müller, F.A., Sturla, S.J., 2019. Human in vitro models of nonalcoholic fatty liver disease. Curr. Opin. Toxicol. 16, 9–16. https://doi.org/10.1016/j.cotox.2019.03.001.
Nishizawa, M., Tsuda, M., Hayashi, K., 1990. Two caffeic acid tetramers having enantiomeric phenyldihydronaphthalene moieties from Macrotomia euchroma. Phytochemistry 29, 2645–2649. https://doi.org/10.1016/0031-9422(90)85204-S.
Nuñez-Durán, E., Aghajan, M., Amrutkar, M., Sütt, S., Cansby, E., Booten, S.L., Watt, A., Ståhlman, M., Stefan, N., Häring, H., Staiger, H., Borén, J., Marschall, H., Mahlapuu, M., 2018. Serine/threonine protein kinase 25 antisense oligonucleotide treatment reverses glucose intolerance, insulin resistance, and nonalcoholic fatty liver disease in mice. Hepatol. Commun. 2, 69–83. https://doi.org/10.1002/hep4.1128.
Ohkawa, H., Ohishi, N., Yagi, K., 1979. Assay for lipid peroxides in animal tissues by thiobarbituric acid reaction. Anal. Biochem. 95, 351–358. https://doi.org/10.1016/0003-2697(79)90738-3.

Paschos, P., Paletas, K., 2009. Non alcoholic fatty liver disease and metabolic syndrome. Hippokratia 13, 9–19. https://doi.org/10.1016/S1665-2681(19)31822-8.

Pei, K., Gui, T., Kan, D., Feng, H., Jin, Y., Yang, Y., Zhang, Q., Du, Z., Gai, Z., Wu, J., Li, Y., 2020. An Overview of Lipid Metabolism and Nonalcoholic Fatty Liver Disease. Biomed. Res. Int. 2020, 1–12. https://doi.org/10.1155/2020/4020249.

Perlman, L., Gottlieb, A., Atias, N., Ruppin, E., Sharan, R., 2011. Combining drug and gene similarity measures for drug-target elucidation. J. Comput. Biol. 18, 133–145. https://doi.org/10.1089/cmb.2010.0213.

Pingitore, P., Sasidharan, K., Ekstrand, M., Prill, S., Lindén, D., Romeo, S., 2019. Human multilineage 3D spheroids as a model of liver steatosis and fibrosis. Int. J. Mol. Sci. 20, 1629. https://doi.org/10.3390/ijms20071629.

Rappaport, N., Twik, M., Plaschkes, I., Nudel, R., Iny Stein, T., Levitt, J., Gershoni, M., Morrey, C.P., Safran, M., Lancet, D., 2017. MalaCards: an amalgamated human disease compendium with diverse clinical and genetic annotation and structured search. Nucleic Acids Res. 45, D877–D887. https://doi.org/10.1093/nar/gkw1012.

Sahib, H.B., Aisha, A.F., Yam, M.F., Asmawi, M.Z., Ismail, Z., Salhimi, S.M., Othman, N. H., Abdul Majid, A.M.S., 2009. Anti-angiogenic and anti oxidant properties of Orthosiphon stamineus Benth. Methanolic leaves extract. Int. J. Pharmacol. 5, 162–167. https://doi.org/10.3923/ijp.2009.162.167.

Saidan, N., Aisha, A., Hamil, M.S., Abdul Majid, A.M.S., Ismail, Z., 2015. A novel reverse phase high-performance liquid chromatography method for standardization of Orthosiphon stamineus leaf extracts. Pharmacognosy Res. 7, 23–31. https://doi.org/10.4103/0974-8490.147195.

Sawada, Y., Yokota Hirai, M., 2013. Integrated LC-MS/MS system for plant metabolomics. Comput. Struct. Biotechnol. J. https://doi.org/10.5936/csbj.201301011.

Schuppan, D., Schattenberg, J.M., 2013. Non-alcoholic steatohepatitis: Pathogenesis and novel therapeutic approaches. J. Gastroenterol. Hepatol. 28, 68–76.

Seyedan, A., Alshawsh, M.A., Alshagga, M.A., Mohamed, Z., 2017. Antiobesity and Lipid Lowering Effects of Orthosiphon stamineus in High-Fat Diet-Induced Obese Mice. Planta Med. 83, 684–692. https://doi.org/10.1055/s-0042-121754.

Smith, G.I., Shankaran, M., Yoshino, M., Schweitzer, G.G., Chondronikola, M., Beals, J. W., Okunade, A.L., Patterson, B.W., Nyangau, E., Field, T., Sirlin, C.B., Talukdar, S., Hellerstein, M.K., Klein, S., 2020. Insulin resistance drives hepatic de novo lipogenesis in nonalcoholic fatty liver disease. J. Clin. Invest. 130, 1453–1460. https://doi.org/10.1172/JCI134165.

Sookoian, S., Pirola, C.J., Valenti, L., Davidson, N.O., 2020. Genetic Pathways in Nonalcoholic Fatty Liver Disease: Insights From Systems Biology. Hepatology 72, 330–346. https://doi.org/10.1002/hep.31229.

Su, R.C., Lad, A., Breidenbach, J.D., Blomquist, T.M., Gunning, W.T., Dube, P., Kleinhenz, A.L., Malhotra, D., Haller, S.T., Kennedy, D.J., Vanella, L., 2019. Hyperglycemia induces key genetic and phenotypic changes in human liver epithelial HepG2 cells which parallel the Leprdb/J mouse model of non-alcoholic fatty liver disease (NAFLD). PLoS One 14 (12), e0225604.

Sumaryono, W., Proksch, P., Wray, V., Witte, L., Hartmann, T., 1991. Qualitative and quantitative analysis of the phenolic constituents from Orthosiphon aristatus. Planta Med. 57, 176–180. https://doi.org/10.1055/s-2006-960060.

Sun, W., Liu, P., Yang, B., Wang, M., Wang, T., Sun, W., Wang, X., Zheng, W., Song, X., Li, J., 2021. A network pharmacology approach: Inhibition of the NF-κB signaling pathway contributes to the NASH preventative effect of an Oroxylum indicum seed extract in oleic acid-stimulated HepG2 cells and high-fat diet-fed rats. Phytomedicine 88,. https://doi.org/10.1016/j.phymed.2021.153498 153498.

Szklarczyk, D., Franceschini, A., Wyder, S., Forslund, K., Heller, D., Huerta-Cepas, J., Simonovic, M., Roth, A., Santos, A., Tsafou, K.P., Kuhn, M., Bork, P., Jensen, L.J., Von Mering, C., 2015. STRING v10: Protein-protein interaction networks, integrated over the tree of life. Nucleic Acids Res. 43, D447–D452. https://doi.org/10.1093/nar/gku1003.

Tezuka, Y., Stampoulis, P., Banskota, A.H., Awale, S., Tran, K.Q., Saiki, I., Kadota, S., 2000. Constituents of the Vietnamese medicinal plant Orthosiphon stamineus. Chem. Pharm. Bull. 48, 1711–1719. https://doi.org/10.1248/cpb.48.1711.

Thomas, P.D., Campbell, M.J., Kejariwal, A., Mi, H., Karlak, B., Daverman, R., Diemer, K., Muruganujan, A., Narechania, A., 2003. PANTHER: A library of protein families and subfamilies indexed by function. Genome Res. 13, 2129–2141. https://doi.org/10.1101/gr.772403.

Trott, O., Olson, A.J., 2010. AutoDock Vina: improving the speed and accuracy of docking with a new scoring function, efficient optimization, and multithreading. J. Comput. Chem. 31, 455–461. https://doi.org/10.1002/jcc.21334.

Xie, X., Miao, J., Sun, W., Huang, J., Li, D., Li, S., Tong, L., Sun, G., 2017. Simultaneous determination and pharmacokinetic study of four phenolic acids in rat plasma using UFLC–MS/MS after intravenous administration of salvianolic acid for injection. J. Pharm. Biomed. Anal. 134, 53–59. https://doi.org/10.1016/j.jpba.2016.10.017.

Yam, M.F., Basir, R., Asmawi, M.Z., Ismail, Z., 2007. Antioxidant and hepatoprotective Effects of Orthosiphon stamineus Benth. Am. J. Chin. Med. 35, 115–126. https://doi.org/10.1142/S0192415X07004679.

Younossi, Z.M., 2019. Non-alcoholic fatty liver disease – A global public health perspective. J. Hepatol. 70, 531–544. https://doi.org/10.1016/j.jhep.2018.10.033.

Yu, L., Qian, J., 2020. Dihydrotanshinone I alleviates spinal cord injury via suppressing inflammatory response, oxidative stress and apoptosis in rats. Med. Sci. Monit. 26. https://doi.org/10.12659/MSM.920738.

Zhang, R., Chu, K., Zhao, N., Wu, J., Ma, L., Zhu, C., Chen, X., Wei, G., Liao, M., 2020. Corilagin alleviates nonalcoholic fatty liver disease in high-fat diet-induced C57BL/6 mice by ameliorating oxidative stress and restoring autophagic flux. Front. Pharmacol. 10. https://doi.org/10.3389/fphar.2019.01693.

Zhou, J., Xie, G., Yan, X., 2011. Encyclopedia of Traditional Chinese Medicines - Molecular Structures, Pharmacological Activities, Natural Sources and Applications, Encyclopedia of Traditional Chinese Medicines - Molecular Structures. In: Pharmacological Activities, Natural Sources and Applications. Springer, Berlin Heidelberg, Berlin, Heidelberg. https://doi.org/10.1007/978-3-642-16735-5.